

# Intraseasonal to interannual variability of zooplankton biomass and standing stock inferred from ADCP backscatter in the eastern Arabian Seas

Ranjan Kumar Sahu<sup>a,b</sup>, D. Shankar<sup>a,b,\*</sup>, P. Amol<sup>b,c</sup>, S.G. Aparna<sup>a,b</sup>, D.V. Desai<sup>a,b</sup>

<sup>a</sup>*CSIR-National Institute of Oceanography, Dona Paula, 403004, Goa, India*

<sup>b</sup>*Academy of Scientific and Innovative Research (AcSIR), Ghaziabad, 201002, Uttar Pradesh, India*

<sup>c</sup>*CSIR-NIO, Regional Centre, Visakhapatnam, 530017, Andhra Pradesh, India*

---

## Abstract

Variation of zooplankton biomass and standing stock in the eastern Arabian Sea (EAS) is mapped using backscatter measurements from 153.3 kHz acoustic Doppler current profiler moorings deployed at seven locations on the continental slope off the west coast of India from October 2017 to December 2023. The conversion from backscatter to biomass is based on volumetric zooplankton sampling. Zooplankton biomass in 24–140 m decreases from the upper ocean to lower depths. Changes are observed in seasonal variation of zooplankton standing stock monthly climatology (24–120 m biomass integral) as we move poleward along the slope. Standing stock variation is lowest at Kanyakumari followed by Okha, each at the southern and northern boundary of EAS, respectively. Analysis reveals that the seasonal variation of zooplankton biomass is comparable to the intraseasonal variability which occurs within a season. Annual cycle is predominant at north-EAS and it decreases towards south-EAS where the semi-annual cycle tends to dom-

---

\*Corresponding author

Email address: [shankar@nio.res.in](mailto:shankar@nio.res.in) (D. Shankar)

inate. Interannual variability, is observed with periods corresponding to  $\sim$ 720 days, moderately off Mumbai and feebly off Goa. The use of seven moorings provides a map of variability along the slope from the southern end of EAS to almost its northern end. Stronger intraseasonal variability has implication on conventional sampling using ship-based methods because of the time it takes to cover EAS regime.

*Keywords:* ADCP backscatter, zooplankton, biomass, standing stock, variability, eastern Arabian Sea

---

## 1. Introduction

### 2 1.1. Background

Zooplankton play a vital role in the food web of pelagic ecosystem by enabling the hierarchical transport of organic matter from primary producers to higher trophic levels, thereby impacting the fish population (Ohman and Hirche, 2001) and the carbon pump of the deep ocean (Quéré et al., 2016). They are presumably the largest migrating organisms in terms of biomass (Hays, 2003) owing to their diel vertical migration (DVM). Zooplankton depend not only on phytoplankton, but also on the microbial loop (Azam et al., 1983); the zooplankton abundance or standing stock therefore depends on environmental variables (e. g., mixed-layer depth or MLD, insolation, oxygen, thermocline, nutrient availability, Chlorophyll-*a* (chl-*a*) concentration, and daily primary production). As is true of the rest of the world ocean, the biological productivity of the north Indian Ocean (NIO; north of 5°N of Indian Ocean) is essentially driven by the physics and chemistry (see, for example, Subrahmanyam, 1959; Banse, 1968, 1995; Ryther et al., 1966; Nair, 1970; Qasim, 1977; Lévy et al., 2007; McCreary et al., 2009; Vijith et al., 2016; Shankar et al., 2016, 2019; Amol et al., 2020), with changing dynamical conditions leading to variations in physico-chemical properties and therefore causing blooms and growth of plankton in favourable conditions. The changes are strongly influenced by the seasonal cycle in the NIO (Banse, 1968; McCreary et al., 1996, 2009; Lévy et al., 2007; Shankar et al., 2019; Aparna et al., 2022). The eastern boundary of the Arabian Sea contains the West India Coastal Current (WICC), which reverses seasonally, flowing poleward (equatorward) during November–February (June–September) (Banse, 1968; Shetye et al., 1990, 1991; Vijith et al., 2022; McCreary et al.,

1993; Shankar and Shetye, 1997; Shankar et al., 2002).

28 A direct consequence of this reversal is the seasonal cycle of the thermocline (Shetye et al., 1990, 1991; Vijith et al., 2022) and oxycline (DeSousa et al., 1996; Schmidt et al., 2020) due to the upwelling (downwelling) favourable conditions during summer (winter) in the eastern Arabian Sea  
30 (EAS; Shetye et al., 1990, 1991; Vijith et al., 2022); the mixed-layer depth (MLD) responds to the changes in the thermocline and the mixing driven  
32 by the local winds and the changes in near-surface stratification (Shetye et al., 1991; Prasad and Bahulayan, 1996; Kumar and Narvekar, 2005). In  
34 response, the phytoplankton biomass and chl-*a* concentration changes with season (Subrahmanyam and Sarma, 1960; Banse, 1968; Kumar and Narvekar,  
36 2005; Lévy et al., 2007; McCreary et al., 2009; Vijith et al., 2016; Shankar et al., 2019). Upwelling during the summer monsoon leads to maximum chl-*a*  
38 growth in the EAS (Banse, 1968; Banse and English, 2000; McCreary et al., 2009; Hood et al., 2017; Bemal et al., 2018; Shi and Wang, 2022). During  
40 the winter monsoon, convective mixing driven by dry winds was considered  
42 the key process leading to the deep mixed layer in the northeastern Arabian  
44 Sea (NEAS) (Banse, 1968; Shetye et al., 1992; Madhupratap et al., 1996b;  
46 McCreary et al., 1996; Lévy et al., 2007), but recent results show that the  
48 poleward advection of warm and fresher water plays a key role in restricting  
50 the deep mixed layers to the northern part of the NEAS (Shankar et al.,  
52 2016). This deepening of the mixed layer leads to a winter chl-*a* peak in the  
NEAS (Madhupratap et al., 1996b; McCreary et al., 1996; Lévy et al., 2007;  
54 Shankar et al., 2016; Vijith et al., 2016; Keerthi et al., 2017; Shi and Wang,  
56 2022). In the southeastern Arabian Sea (SEAS), downwelling Rossby waves  
modulate chl-*a* during the winter monsoon, but this effect is limited to the  
neighbourhood of the coast and islands (Amol et al., 2020); hence, the chl-*a*

54 peak in the SEAS is limited to the summer monsoon.

The zooplankton grazing peak is instantaneous with no time delay from  
55 peak phytoplankton production (Li et al., 2000; Barber et al., 2001), but its  
population growth lags (Rehim and Imran, 2012; Almén and Tamelander,  
56 2020) depending on its gestation period and other limiting aspects. Some  
studies suggest that the peak timing of zooplankton may not change in par-  
58 allel with phytoplankton blooms (Winder and Schindler, 2004), but others  
indicate that a lag exists between primary production and the transfer of en-  
60 ergy to higher trophic levels (Brock and McClain, 1992; Brock et al., 1991).  
Conventional, ship-based zooplankton sampling, which captures only a few  
62 snapshots of the variation, give an incoherent or incomplete understanding  
in terms of spatio-temporal variation of zooplankton (Ramamurthy, 1965;  
64 Madhupratap et al., 1992; Piontkovski et al., 1995; Madhupratap et al.,  
1996a; Wishner et al., 1998; Nair et al., 1999; Barber et al., 2001; Jyothibabu  
66 et al., 2010; Khandagale et al., 2022). Generating a time series of zooplank-  
ton biomass and standing stock is, however, possible with calibrated acoustic  
68 instruments such as the acoustic Doppler current profiler (ADCP) (Edvard-  
sen et al., 2003; Smith and Madhupratap, 2005; Smeti et al., 2015; Kang  
70 et al., 2024). The ADCP, by providing a continuous time series at a high  
temporal resolution, can reveal details of the complex interplay between the  
72 physico-chemical and ecosystem variables (Jiang et al., 2007; Potiris et al.,  
74 2018; Shankar et al., 2019; Aparna et al., 2022; Nie et al., 2023), and has  
76 been used to map zooplankton migration (Inoue et al., 2016; Ursella et al.,  
78 2018, 2021) and their seasonal to annual variation (Jiang et al., 2007; Hobbs  
et al., 2021; Liu et al., 2022; Aparna et al., 2022).

The relationship between ADCP backscatter and the abundance and  
80 size of zooplankton was described by Greenlaw (1979) with mono-frequency

backscatter used to estimate abundance along with knowledge of mean zooplankton size. The popularity of the ADCP as a tool to study temporal and spatial variation of zooplankton biomass increased in the 1990s following the introduction of high-frequency echo sounders (Flagg and Smith, 1989; Wiebe et al., 1990; Batchelder et al., 1995; Greene et al., 1998; Rippeth and Simpson, 1998). The ADCP backscatter has been used to study DVM and the spatial and temporal variability of zooplankton biomass in different marine regions, such as the southwestern Pacific (Smeti et al., 2015), the Lazarev Sea in Antarctica (Cisewski et al., 2010), the Canadian Arctic (Hamilton et al., 2013), and the Corsica Channel in the northwestern Mediterranean Sea (Guerra et al., 2019). With networks of moored buoys deployed across the world ocean to measure currents, the potential use of acoustics for understanding coupled physical and biological processes is, however, yet to be fully exploited (Davis et al., 2019). The first such study to explore the potential of ADCPs in EAS was carried out by Aparna et al. (2022) (A22 hereafter) using ADCP moorings deployed on continental slope off the Indian west coast.

### 98    1.2. Objectives and scope

The network of ADCPs used by A22 to map the seasonal cycle of zooplankton biomass and standing stock was originally deployed on the continental slope off the west coast of India to map the variability of the WICC on time scales ranging from the seasonal to the intraseasonal and to provide a measure of its interannual variability (Amol et al., 2014; Chaudhuri et al., 2020). A22 showed that the zooplankton peaks (and troughs) are influenced by the seasonal movement of the thermocline, the oxygen minimum zone (OMZ), and the MLD. Their analysis showed that the zooplankton stand-

ing stock (ZSS) tends to decrease in the SEAS during the summer monsoon,  
108 when upwelling facilitates an increase in phytoplankton biomass.

A22 used ADCP backscatter data from three moorings, one each located off Mumbai (NEAS), Goa (central-eastern Arabian Sea or CEAS), and Kollam (SEAS). We extend the work of A22 by presenting data from four additional moorings in the EAS and highlight the significant intraseasonal variability of biomass and standing stock revealed by the ADCP data.  
114 The article is organized as follows: datasets and methods employed are described in section 2. Section 3 describes the observed time series and the  
116 climatology of zooplankton biomass and standing stock and their seasonal cycle and variability. A brief discussion on interannual variability in section 4  
118 is followed by a detailed discussion in section 5 on intraseasonal variability, which is a major focus in this study. Section 6 summarises the results and  
120 discusses their implications.

## 2. Data and methods

In this section, we describe the data sets used in this article: the primary data are ADCP backscatter (section 2.1) and zooplankton biomass  
122 (section 2.2), but we also use data on temperature, salinity, MLD, oxygen,  
124 and chl-*a* (section 2.3).

### 126 2.1. The ADCP backscatter time series

The ADCP backscatter forms the primary data set used in this article.  
128 The four additional moorings include one off Kanyakumari (in the SEAS, south of Kollam and on the slope off the southern tip of the Indian mainland), Udupi (just north of the SEAS–CEAS boundary), Jaigarh (north of  
130 Goa in the CEAS), and Okha (north of Mumbai in the NEAS); all these

mooring locations are shown in Fig. 1 and listed in Table 1. The ADCPs are of make Teledyne RD Instruments, upward-looking, and operate at 153.3 kHz. Though the Kanyakumari mooring had been deployed in 2009, the top ADCP had a frequency of 76.8 kHz till January 2016, over two years after the shift to 153.3 kHz off Kollam, Goa, and Mumbai (Chaudhuri et al., 2020). That's why the Kanyakumari mooring was not included in the analysis of A22. We include it in our analysis because it starts in October 2017, when the other three moorings were deployed in the EAS.

The moorings on the west-coast slope are serviced once a year during September–December depending on ship availability. Data was collected at hourly intervals with a 4 m bin size. The echoes at the surface render the data useless within roughly 10% of the transducer's range ( $\sim 20$  m) and this data is therefore discarded. We have followed the methodology laid down in A22 to derive the backscatter time series from ADCP echo intensity. Gaps up to two days are filled using the grafting method of Mukhopadhyay et al. (2017) and the graft-filled backscatter time series is converted to zooplankton biomass.

## 2.2. The zooplankton biomass time series

In situ biomass data from volumetric zooplankton samples are used to convert the backscatter to biomass. The zooplankton samples were collected in the vicinity ( $\sim 10$  km) of the ADCP mooring site twice, once prior to retrieval and again following the deployment of the mooring (table 2). A multi-plankton net (MPN, 100  $\mu\text{m}$  mesh size, 0.5  $\text{m}^2$  mouth area) was used to collect samples in the pre-determined depth ranges; the water volume filtered was calculated by sampling depth range and mouth area. The timing of sample collection was different throughout the MPN hauls owing

158 to its dependence on the time or mooring retrieval, but the depth range  
was standardized from 2020 onwards to the bins over 0–25, 25–50, 50–75,  
160 75–100, and 100–150 m. Following numerous previous studies (A22; Flagg  
and Smith, 1989; Heywood et al., 1991; Jiang et al., 2007), the backscatter  
162 was averaged in the vertical corresponding to the specific bins of MPN haul  
for each site and then linearly regressed with the biomass of respective bins  
164 (Fig. 2). The zooplankton biomass in the euphotic zone concentrates in the  
upper 10 m and this shift to near the surface is pronounced during the night.  
166 Yet, this should not be a concern for the regression as it would simply show  
up as low backscatter at deeper depths during night-time corresponding to  
168 low biomass. It is important to note that the study is carried out using daily  
averaged biomass. Therefore, features associated with DVM are eliminated  
170 (A22; Jiang et al., 2007).

The zooplankton biomass time series (Fig. 3) is created from the above  
172 linear regression. The standing stock is determined by taking the vertical in-  
tegral of biomass over the water column. As in A2, to maintain consistency  
174 in the estimation of standing stock over the time series, only those deploy-  
ments that do not lack data at any depth in the entire range of 24–120 m are  
176 considered for analysis. The lack of data above ~24 m is due to the deviation  
in the vertical position of the ADCP transducer in the water column. In  
178 spite of the care taken to position the instrument (mooring) at ~150–200 m  
(~1050–1100 m) depth, the process of mooring deployment, which is done  
180 from a steaming ship, implies that some deployments are shallower or deeper  
owing to drift caused by floater-buoyancy and anchor-weight imbalance. It  
182 leads to a gap in the data at some mooring sites for some years. For exam-  
ple, off Okha, data is not available for the entire upper 120 m depth for the  
184 second deployment (2018–2019). Data is also unavailable off Jaigarh from

the surface to  $\sim$ 60 m data during 2019–2022 and off Kollam during 2020–  
186 2021 below  $\sim$ 80 m. There are also a few deployments during which no data  
or bad data was recorded, e. g., off Udupi (2020–2021) and Kanyakumari  
188 (2022–2023); such bad data are discarded from standing-stock estimation.

A decrease in biomass with increasing depth is observed at all seven  
190 locations (Fig. 3). To demarcate this expected decrease in biomass from the  
more productive upper ocean to the less productive lower ocean, A22 used  
192 the  $215 \text{ mg m}^{-3}$  biomass contour (called  $z_{215}$ ), and this contour is plotted  
for both daily and monthly time series in Fig. 3; the depth of this contour  
194 is called  $D_{215}$ . The lower biomass in the upper ocean off Kanyakumari and  
Okha, however, led us to use the  $175 \text{ mg m}^{-3}$  for these locations. This  
196 contour, whether  $D_{215}$  or  $D_{175}$ , cannot be plotted when data are missing,  
leading to some gaps in its time series.

198 The biomass decrease with depth, roughly defined as the difference be-  
tween mean biomass at 40 m and 104 m, is highest off Jaigarh and Mumbai,  
200 owing to the higher biomass in upper ocean (Fig. 4, table S1) and lowest  
off Kanyakumari; this biomass decrease in the vertical is comparable at the  
202 other four locations. A22 had reported that the decrease in biomass was  
lower off Kollam compared to Mumbai and Goa.  $D_{215}$ , like the biomass at  
204 40 m or 104 m, shows a seasonal variation: it moves up during the summer  
monsoon, when upwelling occurs, and down during the winter monsoon,  
206 when downwelling occurs. Note, however, that there is striking variation in  
 $D_{215}$  over the years sampled: indeed, the high difference between 40 m and  
208 104 m is due to a few years rather than being a feature of the entire record  
at a given location (Figs. 3,4). The mean and standard deviation of biomass  
210 are shown in table S1. The sites with higher biomass tend to have higher  
variation over time, e. g., Mumbai, Jaigarh, and Kollam.

212 *2.3. Temperature, oxygen, mixed-layer depth, and chlorophyll*

As in A22, in order to compare the changes in ZSS with the vertical movement of the thermocline, we use the monthly temperature climatology of Chatterjee et al. (2012) ( $1^{\circ}$  spatial resolution); the depth of the  $23^{\circ}\text{C}$  isotherm (henceforth, *D23*) is used as a proxy for the thermocline. Following A22, for comparison with the vertical movement of the oxycline, we use the monthly climatology of oxygen from the World Ocean Atlas 2013 (García et al., 2014). The oxygen concentration contour used as a proxy for the oxycline is specific to each site owing to the presence of some locations within the oxygen minimum zone (OMZ) and some locations outside its boundaries in the EAS. We use  $2.1 \text{ ml L}^{-1}$  for Kanyakumari and Kollam,  $3.2 \text{ ml L}^{-1}$  for Okha, and  $1.7 \text{ ml L}^{-1}$  for the other four locations; Kanyakumari, Kollam, and Okha lie outside the OMZ (see Fig. 1), but Okha is ventilated better owing to the intrusion of the Arabian Sea High Salinity Water (ASHSW; Rochford, 1964; Wyrtki et al., 1971) from farther north in the NEAS (Banse and Postel, 2009; Naqvi et al., 2006; Shankar et al., 2016). The MLD in the EAS is of the order of  $\sim 20\text{--}40 \text{ m}$  during the summer monsoon (Shetye et al., 1990; Shankar et al., 2005; Sreenivas et al., 2008), especially in the SEAS (Shenoi et al., 2005), but the MLD remains deep in the northern NEAS during winter (Shankar et al., 2016). As in A22, the climatological MLD is calculated using the temperature and salinity from the Chatterjee et al. (2012) data set using a density criterion: the MLD is defined as the depth at which the density increase from the surface corresponds to a  $0.5^{\circ}\text{C}$  decrease in temperature (Shenoi et al., 2004).

A22 used chl-*a* data from SeaWiFS, but this satellite ended service in 2010; hence, we use the new chl-*a* product from Global Ocean Colour. Biogeochemical Level-3 data is obtained from E. U. Copernicus Marine Service

Information. The daily data is available at a spatial resolution of 4 km,  
240 but, like all satellite chl-*a* data, has gaps owing to clouds. Hence, to ensure  
a continuous climatological time series, after performing grafting method  
242 of Mukhopadhyay et al. (2017) on chl-*a* a trade-off is made between min-  
imizing the gaps in chl-*a* data and retention of at least 10 data points for  
244 computing the 30-day running-mean.

### 3. The seasonal cycle

246 In this section, we discuss the seasonal climatology and the seasonal  
cycle.

#### 248 3.1. Climatology of zooplankton biomass and standing stock

The monthly climatology of biomass, ZSS, and chl-*a* was computed from  
250 the monthly means, which were estimated for every month for which at least  
10 days of data were available. Therefore, since we have used all the available  
252 data at each location, the number of years for which the average is computed  
is not the same at all locations because there are some gaps at some loca-  
254 tions (Okha, for example). Yet, the similar behavior of the A22 climatology  
(2012–2020) and our climatology (2018–2023) off Kollam, Goa, and Mumbai  
256 suggests that the basic features are strong aspects of the seasonal climatol-  
ogy (see section S1). Such strong features include the following (Fig. S1):  
258 the decrease in zooplankton biomass from the upper ocean to below *D*215 is  
weaker off Kollam compared to Goa and Mumbai; there is high ZSS during  
260 the winter monsoon at all three locations in the EAS; there is a mismatch  
in the chl-*a* peak, which occurs during the summer monsoon, and the ZSS  
262 peak, which occurs during the winter monsoon, off Kollam. While some  
other details may vary between the two climatologies (higher zooplankton

<sup>264</sup> biomass off Kollam and lower biomass off Goa in the new climatology), the  
<sup>265</sup> basic features are consistent. We can infer that phytoplankton dominate in  
<sup>266</sup> the SEAS and the microbial loop in the NEAS, a conclusion reached by both  
<sup>267</sup> A22 and Shankar et al. (2019), which allowed the latter to infer explain why  
<sup>268</sup> planktivorous (carnivorous) fish like the oil sardine dominate in the SEAS  
(NEAS).

<sup>270</sup> The four additional moorings throw more light on this transition from  
<sup>271</sup> a phytoplankton-dominated ecosystem in the SEAS to a microbial-loop-  
<sup>272</sup> dominated ecosystem in the NEAS. We find a decrease in chl-*a* from Kollam  
<sup>273</sup> ( $0.64 \text{ mg m}^{-3}$ ) to Jaigarh ( $0.27 \text{ mg m}^{-3}$ ) and an increase farther north in the  
<sup>274</sup> NEAS (Fig. 5, table S2). The change in the range or standard deviation (SD)  
<sup>275</sup> of chl-*a* is, however, much more striking from Kollam to Okha: the range  
<sup>276</sup> decreases from  $2.26 \text{ mg m}^{-3}$  off Kollam to a negligible value of  $0.15 \text{ mg m}^{-3}$   
<sup>277</sup> off Jaigarh before increasing again to  $0.72 \text{ mg m}^{-3}$  off Okha. Therefore,  
<sup>278</sup> chl-*a* and the range of its variation are weaker in the CEAS and increase  
<sup>279</sup> on either side of Jaigarh. The variation of ZSS is in striking contrast to  
<sup>280</sup> the variation of chl-*a*. The mean ZSS decreases from Kollam ( $24.6 \text{ g m}^{-2}$ )  
<sup>281</sup> to Goa ( $21.2 \text{ mg m}^{-2}$ ), but increases to  $24.2 \text{ g m}^{-2}$  (practically the same  
<sup>282</sup> as off Kollam) off Jaigarh before decreasing farther north. The range of  
<sup>283</sup> ZSS variation, however, increases over twofold from  $4.1 \text{ g m}^{-2}$  off Kollam to  
<sup>284</sup>  $9 \text{ g m}^{-2}$  off Jaigarh before decreasing again farther north. So the conclusion  
<sup>285</sup> of a phytoplankton-dominated (microbial-loop-dominated) ecosystem in the  
<sup>286</sup> SEAS (NEAS) inferred by A22 is strengthened by the new climatology:  
<sup>287</sup> the transition tends to occur in the CEAS and can be considered to occur  
<sup>288</sup> roughly north of Udupi owing to the significant decrease in the range of chl-*a*  
from Udupi to Goa.

<sup>290</sup> The mooring location off Kanyakumari is distinct from the other six

mooring locations because the former lies at the junction of the Bay of Bengal and the Arabian Sea, in the regime of the seasonally reversing monsoon-current system (Shankar et al., 2002); the other six moorings lie on the slope off the Indian west coast. Therefore, we excluded Kanyakumari from the above discussion of chl-*a* and ZSS variation along the west-coast slope. This change in location *vis-a-vis* the west coast is seen in the chl-*a* and ZSS variation off Kanyakumari, where we find a high range of chl-*a* about a high mean chl-*a*, while the ZSS shows a low range of variation about a low mean value (Fig. 5, table S2). Off Jaigarh, in contrast, we find a high range of ZSS and a negligible range of chl-*a* about a low mean chl-*a*.

### 3.2. Seasonal cycle and variability

This seasonal cycle is evident in the time series (Fig. 4) and in the wavelet power spectra (see section S2 for a brief discussion of wavelet analysis) of the biomass at 40 m and 140 m (Fig. 6) and the ZSS (Fig. 7). It is also seen in the biomass filtered in the seasonal band (see section S2 for a brief discussion of filtering) of 100-400 days (Fig. 8) to extract only the seasonal variability, i. e., variability at a period of over three months so that it can be captured to an extent in a monthly time series. The wavelet spectra of biomass (Fig. 6) show high variability, denoted by the reddish colours, at all locations, but the strength of this variability is not the same at all locations. Off Kanyakumari, for example, the variability in the seasonal band is low, as indicated by the colour at both depths; in contrast, the seasonal variability appears strong in the wavelet spectra off Goa and Mumbai. In the filtered plot (Fig. 8), this change from Kanyakumari to Jaigarh is seen in the weaker shades of red and blue off Kanyakumari compared to the deeper shades off Jaigarh. The utility of the wavelet spectrum and the filtered biomass lies,

however, in their ability to show how this seasonal variability changes over  
318 time. For example, the change in shades shows that the seasonal cycle is weak in both the wavelet spectrum of biomass at 40 m and the filtered  
320 biomass off Kollam during 2020 and increases from 2021 onwards off Goa.

Note also that the colour often switches from red (positive change from  
322 the mean) to blue (negative change from the mean) around  $D175$  or  $D215$  (Fig. 8), which are defined using the monthly time series of biomass, pointing  
324 to the role of this contour in separating the upper and lower ocean with respect to the zooplankton biomass. When such a change of colour occurs,  
326 the positive change and negative change on either side of the curve cancel each other in the vertical integral to determine ZSS. Hence, since such a  
328 change across  $D175$  is seen frequently off Kanyakumari, the ZSS at this location shows a negligible variation, leading to a low SD in the climatology  
330 (Fig. 5, table S2).

Another feature noted by A22 and striking in the climatological ZSS  
332 (Fig. 5) is the asymmetry in time: the increase from the minimum during the summer monsoon occurs much faster than the decrease from the maximum  
334 during the winter monsoon. A consequence of this asymmetry is the presence of significant variability at the semi-annual period ( $\sim 180$  days) in addition to  
336 the annual period ( $\sim 365$  days): this variability has been noted earlier in the west-coast alongshore currents (Amol et al., 2014; Chaudhuri et al., 2020).  
338 Amol et al. (2014) split the seasonal variability of the current in the 100–400-day period band (see section S2) into two distinct bands, the annual  
340 band in the period range 300–400 days and the intra-annual band in the period range 100–250 days. The wavelet spectra show that the variability in  
342 the intra-annual band of  $\sim 100$ –250 days is not confined to the semi-annual period of 180 days, but extends to lower periods within this band. In the

<sup>344</sup> currents, variability around  $\sim$ 120 days has been noted (Amol et al., 2014;  
<sup>345</sup> Chaudhuri et al., 2020) and variability around this period is also seen in the  
<sup>346</sup> biomass (Fig. 6) at some locations. For example, off Kollam, the wavelet  
<sup>347</sup> spectrum at 40 m shows variability around  $\sim$ 180 days in 2019–2020, but it  
<sup>348</sup> is stronger at lower periods within this intra-annual band in 2021–2022. In  
<sup>349</sup> general, the annual band for zooplankton biomass tends to be weaker than  
<sup>350</sup> the intra-annual band (Figs. 6,S2). Even within the weak seasonal cycle off  
<sup>351</sup> Kanyakumari, variability is stronger in the intra-annual band compared to  
<sup>352</sup> the annual band (Fig. S2).

#### 4. Interannual variability

<sup>354</sup> Interannual variability of the monthly time series may be considered to  
<sup>355</sup> occur in two ways. First, there can be years in which the biomass or ZSS  
<sup>356</sup> changes in one direction throughout the year, implying a significant devia-  
<sup>357</sup> tion from the seasonal cycle, but at a period clearly different from variability  
<sup>358</sup> within a season. Second, there can be a variability that is captured at a pe-  
<sup>359</sup> riod higher than a year in a Fast Fourier Transform (FFT) or a wavelet  
<sup>360</sup> spectrum.

The first kind of interannual variability is obvious from a comparison of  
<sup>362</sup> the biomass climatology (Fig. 5) and the biomass time series (Fig. 3). It  
<sup>363</sup> is clear, for example, that the high climatological biomass above *D215* off  
<sup>364</sup> Kollam during the summer monsoon is due to the high biomass occurring  
<sup>365</sup> during a few years: the red colour is seen in 2022 and to a lesser extent in  
<sup>366</sup> 2021 and 2023, but it is missing in earlier years. A more striking case occurs  
<sup>367</sup> during 2020, when the biomass off Kollam collapsed over the entire depth  
<sup>368</sup> range of sampling (Fig. 3; see section S3) and this lower biomass is clearly

seen in the biomass curves at 40 m and 140 m (Fig. 4). A consequence of this  
370 collapse in zooplankton biomass is the significantly lower ZSS during 2020  
off Kollam (Fig. 4). Such deviations, but usually of a weaker magnitude,  
372 from the expectation of the seasonal climatology occur fairly frequently at  
all locations. Off Goa, the climatology of A22 shows higher biomass above  
374 D215 than does the new climatology (Fig. S1); an examination of the data  
for 2012–2020 shows lower biomass during the summer monsoon in most of  
376 the years sampled in the new climatology compared to that of A22, leading  
to lower power around the annual band ( $\sim$ 360 days) in the wavelet spectrum  
378 in the second half of the record (Fig. 9).

The second kind of interannual variability requires a change that occurs  
380 over more than a year. A22 noted the presence of this second kind of inter-  
annual variability off Kollam: the wavelet spectrum showed high power in a  
382 band around 720 days or roughly two years, but it was outside the wavelet  
cone of influence (see section S2), implying that the time series was too short  
384 for the seeming quasi-biennial oscillation (QBO; Mooley and Parthasarathy,  
1984; Bhalme et al., 1987), a well-known signal in Indian monsoon rainfall  
386 and therefore of monsoon variability, to be statistically significant. The per-  
sistent signal did, however, suggest a longer record would prove its existence  
388 off Kollam. An examination of the wavelet spectrum over 2012–2023 shows  
a strong signal at this period during 2012–2018 (Fig. 9), but it weakens af-  
390 ter that and the interannual band seems to shift to higher periods (Fig. 9).  
The QBO signal is also seen off Mumbai in the middle of the record, but  
392 appears at a higher period before 2017 and after 2021; it is weaker off Goa  
and appears outside the cone of influence (Fig. 9).

394 **5. Intraseasonal variability**

Apart from interannual variability, A22 also commented on the existence of intraseasonal variability in the daily biomass data obtained from the ADCP backscatter.

398 *5.1. The wavelet spectrum*

Though they did not analyse it, A22 pointed out that this variability within a season is not small: indeed, that this intraseasonal variability is strong is clearly seen in the deviation of the light-coloured curves for the daily data from the darker curves for the 30-day running mean of the biomass at 40 m and 104 m and in the ZSS (Fig. 4). These significant deviations lead to a clear signal in the wavelet power at periods below 90 days for the 40 m and 104 m biomass (Fig. 6). Unlike the wavelet power at the seasonal time scales, which tends to be continuous in, say, the annual band for a year or more, the intraseasonal wavelet power is patchy; such patchiness in the intraseasonal wavelet spectrum also holds for the currents (Amol et al., 2014; Mukherjee et al., 2014; Chaudhuri et al., 2020; Mukhopadhyay et al., 2020). This patchiness is a consequence of the intraseasonal biomass bursts not occurring throughout the year or the time series, but on occasions within a season. The intraseasonal variability is prominent in the 30–90-day band in the wavelet power spectrum, but there is also variability at periods shorter than 30 days (Fig. 6). For the currents, the lower bound used was  $\sim 5$  days in order to filter out inertial currents off Kanyakumari, which has the highest inertial period of the seven locations (Amol et al., 2014; Chaudhuri et al., 2020). We retain this lower limit for our analysis of the intraseasonal variability of biomass and ZSS, i. e., we define the intraseasonal variability to occur in the period range of 5–90 days, with the 30–90-day (5–30-day) band constituting

<sup>420</sup> the “low-frequency” (“high-frequency”) parts of the intraseasonal spectrum;  
<sup>421</sup> the low-frequency part of this band is marked by the horizontal lines in the  
<sup>422</sup> wavelet plots.

The wavelet power is not normalised in this analysis. Therefore, even if  
<sup>424</sup> the amplitude is the same at two different periods, the wavelet power will  
be less for the higher frequency ([https://paos.colorado.edu/research/  
426 wavelets/faq.html](https://paos.colorado.edu/research/wavelets/faq.html)). Hence, we cannot infer from the red (yellow) colours  
for the seasonal (intraseasonal) band in the wavelet spectrum (Fig. 6) that  
<sup>428</sup> variability is higher in the seasonal band. Though this limitation of the  
wavelet spectrum can be overcome by normalising the wavelet power, we  
<sup>430</sup> prefer to apply band-pass filters to extract the variability in the intraseasonal  
band (Fig. 10), as done earlier for the seasonal cycle (Fig. 8), because the  
<sup>432</sup> result of this filtering is more intuitive.

### *5.2. Range of intraseasonal variability*

<sup>434</sup> Filtering the biomass with a band-pass filter (Fig. 10) suggests that the  
biomass range in the 5–90-day or intraseasonal band is comparable to that  
<sup>436</sup> in the seasonal band (Fig. 8) and it often exceeds the seasonal range. (As  
noted earlier for the filtered plot of the seasonal cycle, the filtered intrasea-  
<sup>438</sup> sonal biomass shows the deviation from the mean, leading to both positive  
(red) and negative (blue) values.) The short time scale associated with the  
<sup>440</sup> intraseasonal band makes it difficult to draw inferences from a plot of the  
entire time series (Fig. 10); hence, we present the analysis for 2019. This  
<sup>442</sup> year is chosen because this deployment was not at the beginning or end  
of the time series (See section S2 for the impact of filtering at the ends of  
<sup>444</sup> the time series.) and there are fewer data gaps in the daily biomass time  
series. Note that our interest here is limited to showing that there is strong

<sup>446</sup> intraseasonal variability in zooplankton biomass, not in the details of this  
variability for any year (including 2019). Hence, we show only the 2019 fig-  
<sup>448</sup> ure for Kollam here (Fig. 11); the figures for the other locations are available  
in the supplement (Figs. S4–S9).

<sup>450</sup> The expanded time axis shows that the range of biomass at 40 m in the 5–  
90-day band (Fig. 11b) is comparable to that in the seasonal band (Fig. 11a)  
<sup>452</sup> off Kollam. There are, however, significant periods when intraseasonal vari-  
ability is weak (lighter shades of blue and red in Fig. 11b); these relatively  
<sup>454</sup> quiescent periods are compensated by the occasions on which the intrasea-  
sonal range is significantly higher than the seasonal range (Fig. 11a,b,c). The  
<sup>456</sup> daily biomass at 40 m is therefore determined by significant contributions  
from both seasonal and intraseasonal bands, with the relative contributions  
<sup>458</sup> changing through the year: strong intraseasonal bursts lasting roughly a  
month are seen from the end of July through October (Fig. 11c). This re-  
<sup>460</sup> sult, that the range of intraseasonal variability is comparable to the seasonal  
range, holds for the rest of the time series off Kollam (Figs. 8,10), leading  
<sup>462</sup> to the SD for both bands being comparable at 40 m (table S3). The same  
comparison holds off Udupi (Figs. 10,S5, table S3), which lies just north of  
<sup>464</sup> the boundary between the SEAS and the CEAS. Off Kanyakumari, how-  
ever, the significantly weaker seasonal cycle (Figs. 8) leads to a higher range  
<sup>466</sup> (Fig. S4) and SD (table S3) for the intraseasonal band. The higher range of  
the intraseasonal band is also evident off Goa (Fig. S6) and Jaigarh (Fig. S7)  
<sup>468</sup> in the CEAS (Fig. 10, table S3). A stronger seasonal cycle compared to the  
CEAS implies that range of the seasonal and intraseasonal bands is again  
<sup>470</sup> comparable off Mumbai (Fig. S8, table S3). Off Okha, the data gaps imply  
that the filled part of the seasonal band is small (Fig. 8); hence, it is difficult  
<sup>472</sup> to attach much significance to the higher intraseasonal range indicated by

the high SD in this band (table S3).

474 At 104 m, i. e., below  $D215$  or  $D175$ , the range of the intraseasonal  
band is less than at 40 m off Kanyakumari (Fig. S4c), Kollam (Fig. 11c),  
476 and Udupi (Fig. S5c), i. e., in the SEAS (table S3). The range at both depths  
is comparable at the other locations. The intraseasonal range is higher than  
478 the seasonal range off Kanyakumari and Jaigarh, lower than the seasonal  
range off Udupi, and of a similar magnitude at the other locations, including  
480 Kollam (Figs. 8,10,11,S4–S9, table S3). Therefore, even the non-monotonic  
pattern that is suggested by the data at 40 m is not applicable at 104 m.

482 *5.3. Spikes in biomass*

Striking at both 40 m and 104 m, however, is the seemingly higher range  
484 of the daily biomass than is indicated by a mental addition of the biomass  
in the seasonal and intraseasonal bands (Figs. 11c,S4c–S9c). Part of this  
486 difference may be due to interannual variability, i. e., biomass varying at  
periods higher than  $\sim 400$  days. Therefore, we applied a 5-day low-pass  
488 filter to the biomass to include this variability at time scales longer than  
the seasonal and compared it with the daily biomass (Figs. 11d,S4d–S9d).  
490 The two curves almost overlap, suggesting that almost the entire variability  
of the daily biomass curve at any depth can be explained by adding the  
492 variability in the intraseasonal, seasonal, and interannual bands. The slight  
difference between the black and red curves (blue and cyan curves) for the  
494 low-passed and daily biomass at 40 m (104 m) suggests, however, that there  
is some variability at periods shorter than 5 days. An example of such a  
496 difference at 40 m occurs towards the end of July off Kollam (Fig. 11d).

Subtracting the 5-day low-passed biomass from the daily biomass shows  
498 the existence of spikes in the daily biomass (Figs. 11e,S4e–S9e). On several

occasions, these spikes exceed one SD (dark grey background) and they  
500 exceed two SD (light grey background) on a few occasions. Examples of  
spikes exceeding two SD at 40 m are seen towards the end of July and  
502 August and in September off Kollam (Fig. 11e). Similar spikes are seen in  
the biomass at 104 m, but fewer of these spikes exceed one SD or two SD.  
504 Such spikes, which extend the peaks in the daily biomass above the sum  
of the seasonal and intraseasonal bands, are also evident at the other six  
506 locations (Figs.S4e–S9e); the largest spikes occur at both 40 m and 104 m  
off Jaigarh (Fig. S7e). These spikes, particularly in comparison to one SD,  
508 occur at random throughout the year. Analysis shows that these spikes are  
not caused by an abnormal change in the DVM; when these spikes occur,  
510 the daily biomass increases (decreases) throughout the day for a positive  
(negative) spike.

#### 512 5.4. Variation in the vertical and standing stock

The variability in the intraseasonal band tends to be weaker below  $D215$   
514 or  $D175$ , implying weaker variability at 104 m compared to 40 m (Fig. 6),  
but there are occasions on which the deviation is stronger at 104 m than  
516 at 40 m (Fig. 10); this strong variation below  $D215$  is seen in the CEAS  
and NEAS, with December 2020 to January 2021 providing one such in-  
518 stance off Mumbai (Figs. 6,10). There are also occasions when high vari-  
ability in the 30–90-day band is seen at both depths in the wavelet spectrum  
520 (Fig. 6) and in the filtered biomass (Fig. 10); an example is during August–  
November 2018 off Udupi, Goa, and Jaigarh in the CEAS. Variability in this  
522 band is also seen off Kollam and Mumbai during August–November 2018,  
but it is clearly weaker and more short-lived (Figs. 6,10).

524 The response of biomass in seasonal scale is positive for both the depths

only during October, indicating even at seasonal scale, it's not necessary that  
526 the biomass in entire water column responds the same way at all the depths.  
Together (Fig. 11b) they determine low-frequency variabilities greater than  
528 5 days seen in biomass and ZSS (Fig. 11e).

As expected, the ZSS tends to be high when the variation above and  
530 below  $D215$  or  $D175$  is in the same direction. Intraseasonal peaks in biomass  
and also in ZSS are strong in the SEAS, comparatively weaker in the CEAS,  
532 and weakest in the NEAS (Fig. 10, table S3).

## 6. Discussion

### 534 6.1. Summary

We present the ADCP backscatter-derived zooplankton biomass time se-  
536 ries across distinct regimes of the EAS from 2017 to 2023. The extended  
dataset, now including four additional stations, offers a clearer view of tran-  
538 sitions in biomass levels and variability. Climatology shows higher biomass  
during the summer monsoon in SEAS and during the winter monsoon in  
540 NEAS, with a gradual transition of peak biomass along CEAS (Section 3.1).

A strong decline in biomass with depth is observed off Goa, followed by  
542 Jaigarh, and then across NEAS and SEAS locations. The minor peak in ZSS  
off Mumbai, noted in A22's climatology, is absent in the updated dataset.  
544 The EAS regime is characterized by a complex combination of biomass vari-  
abilities. The annual cycle results in biomass peaks during the winter (sum-  
546 mer) monsoon and a deeper  $D215$  off NEAS (SEAS) (Fig. 7). The transition  
of biomass and ZSS from NEAS to the SEAS is led by a stronger semi-annual  
548 cycle, interannual variation, and prominent intraseasonal variability as we  
go equatorward.

550        The presence of intraseasonal variability is marked by bursts rolling over  
few weeks to standalone spikes lasting less than 5 days. We categorized the  
552        intraseasonal variability to two distinct intervals, 30–90-day (low frequency)  
and 5–30-day (high frequency) (Fig. 11,Figs. S4–S9). Notably, combined in-  
554        traseasonal variability between 5–90-day band is comparable to, and at times  
exceeds, seasonal fluctuations and it shows a northward decline in surface  
556        biomass (table S3). Biomass fluctuations at 40 m are generally stronger than  
at 104 m, though exceptions exist, especially in the CEAS and NEAS and  
558        it is reflected in the ZSS (table S4, last column). The ZSS shows no such  
pattern like surface biomass as there is reduction/enhancement of ZSS on  
560        account of out-of-phase/in-phase upper and lower depth biomass occurring  
at annual, intra-annual and intraseasonal time scales (Fig. S3). Regional  
562        patterns show strongest intraseasonal signals in the SEAS, moderate in the  
CEAS, and weakest in the NEAS. Biomass variability with period less than  
564        5 days indicates sharp spikes that are not captured by seasonal or intrasea-  
sonal filters. These spikes are suggestive of alternative food chain necessary  
566        for sustenance, and rapid growth or decline of the zooplankton biomass.

### *6.2. Role of the physical forcing*

568        High SLA coincides with lower 40 m biomass. Low in SLA coincides  
with higher 40 m biomass. Fig. 11d

570        The daily biomass at 40 m and 104 m tends to be of same range, but  
differ drastically during May to September when the sea level anomaly (SLA)  
572        is lower (Fig. 11, c), high (low) SLA coinciding with lower (higher) 40 m  
biomass.

574        Nevertheless, though the variability in the CEAS during August–November 2018  
appears similar at multiple locations, the wavelet coherence (see section S2)

576 for adjacent moorings is not statistically significant during August–November  
2018.

578 *6.3. The microbial loop*

Fig. 9 RHS

580 Note that the spikes are not seen only during periods of high chl-*a* but  
also at those duration when chl-*a* is low such as during non-monsoon months  
582 when chl-*a* is low. This holds true for rest of the locations as well. For  
example off Kollam during late October, a higher than 2 SD difference in the  
584 104 m daily and 5-day low-pass filtered biomass is seen off Kollam (Fig. 11,  
d) when chl-*a* is very low. These high-frequency variability points to the  
586 role of microbial loop working in the background and providing sustenance  
for such variations to occur. On the other hands, high spikes are not seen  
588 necessarily only during high chl-*a* e.g., Off Okha during February to April  
(Fig SX), but occurs through out the record and the spikes in chl-*a* doesn't  
590 have to coincide with spike in the difference of daily and 5-day low-pass  
filtered biomass. This is truer for places like Jaigarh (Figs. SX) where the  
592 chl-*a* variation is non-existent, and the biomass has not only high-frequency  
fluctuation but shows clear sign of seasonal variation in ZSS (Fig. 5, c2) and  
594 biomass. These variations are inexplicable without invoking the microbial  
loop that plays important role behind the scene. However, classical food  
596 chain seem to be followed where upwelling is very strong such as in SEAS  
e.g., Kanyakumari 40 m biomass follows the daily chl-*a* pattern (Figs. SX)  
598 during July 2019 but the fluctuation in difference of daily and 5-day low-pass  
filtered biomass is still present.

600 They are present even when chl-*a* is low e.g., year round except monsoon  
time off Kollam, Kanyakumari, indicating role of microbial loop in sus-

602 nance and possible role in the high-frequency (less than 5 day) variability  
seen in the zooplankton biomass.

604 The spikes in background signal S doesn't necessarily coincide with spikes  
or blooms in Chl-a, implying that the spikes in biomass in daily basis doesn't  
606 arise from chl-a but from the functioning of microbial loop. This is truer  
for the cases like Jaigarh, where chl-a variation is non-existent, nonetheless  
608 a seasonal cycle is observed for biomass and ZSS.

610 The classical food web is still active and sometimes dominant in deter-  
mining the surface ocean biomass as seen in Kanyakumari during July 2019  
even though the background signal is present.

#### 612 *6.4. Caveats and strengths*

The results presented in this paper are based on the ADCP backscatter,  
614 which is suitable for creating long-term time series of zooplankton biomass  
in the open ocean (Jiang et al., 2007; Hobbs et al., 2021; Ursella et al., 2021;  
616 Aparna et al., 2022). There are, however, certain limitations to this ap-  
proach of studying biomass using ADCP backscatter as a proxy. While the  
618 variation in depth is captured with in-situ samples from MPN, the varia-  
tion in season is not adequately addressed owing to the limitation of months  
620 when ADCP servicing cruises are undertaken apart from availability. The  
west coast cruises for ADCP servicing are planned for the monsoon transi-  
622 tion months but may start as early as late September till December with  
few exceptions, such as in 2022 when it was carried out in March. Since  
624 the intraseasonal and intra-annual variability is almost double that of the  
annual one (Section 5), the sampling done in a particular season for biomass-  
626 backscatter comparison isn't sufficient but can be mitigated with extensive  
season-wise sampling (Jadhav and Smitha, 2024). However, in their study,

628 the difference in biomass between seasons was about  $15 \text{ mg m}^{-3}$  which is  
comparable to the error bar associated with our backscatter-biomass linear  
630 regression equation. The second limitation is the lack of any information  
regarding the size distribution of zooplankton and their contribution to ZSS  
632 is lost.

The merits outshine the above-mentioned disadvantages in the unique  
634 aspect that a sufficiently long and continuous time series of zooplankton  
biomass could be constructed upon which further analysis can be carried  
636 out. Along with the discussion on seasonal and further climatological cy-  
cles, we provided evidence of strong intraseasonal variation; this has three  
638 major implications: 1) on the conventional sampling methods used to assess  
the zooplankton biomass and standing stock, and the snapshots provided  
640 by such samples aren't representative of a season; 2) on the zooplankton  
patchiness, and further on the under- or overestimation of standing stock;  
642 3) on the predictability, which is reduced due to strong biomass variation at  
intraseasonal scale and the presence of patchiness as spikes and bursts. The  
644 possible influence of ocean currents could be explored using the current data  
from ADCPs (Hitchcock et al., 2002; Lawson et al., 2004). It is evident that  
646 a mono-frequency ADCP is adequately suitable to capture the intraseasonal  
variations of zooplankton biomass that will otherwise be left inaccessible by  
648 traditional methods.

## 7. Declaration of competing interest

650 The authors declare that they have no known competing financial in-  
terests or personal relationships that could have appeared to influence the  
652 work reported in this paper.

## 8. Acknowledgments

654 The present work has been funded by CSIR (Council of Scientific and  
655 Industrial Research, New Delhi, India) and INCOIS (Indian National Cen-  
656 tre for Ocean Information Services, Hyderabad, India) under the COSINE  
(Current Observations and Simulations in the Indian EEZ) project as part  
658 of OSMART Programme. Support of the mooring division and ship cell  
659 of CSIR-NIO is acknowledged for their contribution. Ranjan Kumar Sahu  
660 expresses his acknowledgment to the Council of Scientific and Industrial  
661 Research (CSIR) for sponsoring his fellowship. Additionally, he extends his  
662 thanks to Mr. Ashok Kankonkar for providing the essential data, Mr. Rahul  
663 Khedekar for his help in processing backscatter data, Mr. Roshan D'Souza  
664 for his contribution in processing of zooplankton data. Their contributions  
665 were invaluable to the successful completion of our research. This is NIO  
666 contribution number xxxx.

## References

- 668 Almén, A.K., Tamelander, T., 2020. Temperature-related timing of the  
669 spring bloom and match between phytoplankton and zooplankton. Mar.  
670 Biol. Res. 16, 674–682. [10.1080/17451000.2020.1846201](https://doi.org/10.1080/17451000.2020.1846201).
- 672 Amol, P., Bemal, S., Shankar, D., Jain, V., Thushara, V., Vijith, V., Vinay-  
673 achandran, P.N., 2020. Modulation of chlorophyll concentration by down-  
674 welling Rossby waves during the winter monsoon in the southeastern  
Arabian Sea. Prog. Oceanogr. 186, 102365. [10.1016/j.pocean.2020.102365](https://doi.org/10.1016/j.pocean.2020.102365).
- 676 Amol, P., Shankar, D., Fernando, V., Mukherjee, A., Aparna, S.G., Fer-

- nandes, R., Michael, G.S., Khalap, S.T., Satelkar, N.P., Agarvadekar,  
678 Y., Gaonkar, M.G., Tari, A.P., Kankonkar, A., Vernekar, S., 2014. Observed intraseasonal and seasonal variability of the West India Coastal  
680 Current on the continental slope. *J. Earth Syst. Sci.* 123, 1045–1074.  
10.1007/s12040-014-0449-5.
- Aparna, S.G., Desai, D.V., Shankar, D., Anil, A.C., Dora, S., Khedekar,  
682 R.R., 2022. Seasonal cycle of zooplankton standing stock inferred from  
684 ADCP backscatter measurements in the eastern Arabian Sea. *Prog. Oceanogr.* 203, 102766. 10.1016/j.pocean.2022.102766.
- Azam, F., Fenchel, T., Field, J.G., Gray, J.S., Meyer-Reil, L.A., Thingstad,  
686 F., 1983. The ecological role of water-column microbes in the sea. *Estuaries* 10, 257–263. 10.3354/meps010257.
- Banse, K., 1968. Hydrography of the Arabian Sea shelf of India and Pak-  
690 istan and effects on demersal fishes, in: Deep-Sea Res. Oceanogr. Abstr.,  
Elsevier. pp. 45–79. 10.1016/0011-7471(68)90028-4.
- Banse, K., 1995. Zooplankton: pivotal role in the control of ocean pro-  
692 duction: I. Biomass and production. *ICES J. Mar. Sci.* 52, 265–277.  
694 10.1016/1054-3139(95)80043-3.
- Banse, K., English, D.C., 2000. Geographical differences in seasonality of  
696 CZCS-derived phytoplankton pigment in the Arabian Sea for 1978–1986.  
Deep-Sea Res. Part II Top. Stud. Oceanogr. 47, 1623–1677. 10.1016/  
698 S0967-0645(99)00157-5.
- Banse, K., Postel, J.R., 2009. Wintertime convection and ventilation of the

- 700 upper pycnocline in the northernmost Arabian Sea. *Geophysical Monograph Series* 185, 87–117. [10.1029/2008GM000704](https://doi.org/10.1029/2008GM000704).
- 702 Barber, R.T., Marra, J., Bidigare, R.C., Codispoti, L.A., Halpern, D., John-  
son, Z., Latasa, M., Goericke, R., Smith, S.L., 2001. Primary productivity  
704 and its regulation in the Arabian Sea during 1995. *Deep-Sea Res. Part 2*  
Top. Stud. Oceanogr. 48, 1127–1172. [10.1016/S0967-0645\(00\)00134-X](https://doi.org/10.1016/S0967-0645(00)00134-X).
- 706 Batchelder, H.P., VanKeuren, J.R., Vaillancourt, R.D., Swift, E., 1995.  
Spatial and temporal distributions of acoustically estimated zooplankton  
708 biomass near the marine light-mixed layers station ( $59^{\circ}30'N$ ,  $21^{\circ}00'W$ ) in  
the north Atlantic in May 1991. *J. Geophys. Res. Oceans* 100, 6549–6563.  
710 [10.1029/94jc00981](https://doi.org/10.1029/94jc00981).
- 712 Bemal, S., Anil, A.C., Shankar, D., Remya, R., Roy, R., 2018. Picophy-  
toplankton variability: Influence of winter convective mixing and ad-  
vection in the northeastern Arabian Sea. *J. Mar. Syst.* 180, 37–48.  
714 [10.1029/2001GL013422](https://doi.org/10.1029/2001GL013422).
- 716 Bhalme, H.N., Rahalkar, S.S., Sikder, A.B., 1987. Tropical quasi-biennial  
oscillation of the 10-mb wind and Indian monsoon rainfall — implications  
for forecasting. *J. Climatol.* 7, 345–353. [10.1002/joc.3370070403](https://doi.org/10.1002/joc.3370070403).
- 718 Brock, J.C., McClain, C.R., 1992. Interannual variability in phytoplankton  
blooms observed in the northwestern Arabian Sea during the southwest  
720 monsoon. *J. Geophys. Res. Oceans* 97, 733–750. [10.1029/91JC02225](https://doi.org/10.1029/91JC02225).
- 722 Brock, J.C., McClain, C.R., Luther, M.E., Hay, W.W., 1991. The phy-  
toplankton bloom in the northwestern Arabian Sea during the south-

- west monsoon of 1979. *J. Geophys. Res. Oceans* 96, 20623–20642.  
724 10.1029/91JC01711.
- Chatterjee, A., Shankar, D., Shenoi, S.S.C., Reddy, G.V., Michael, G.S.,  
726 Ravichandran, M., Gopalkrishna, V.V., RamaRao, E.P., UdayaBhaskar,  
T.V.S., Sanjeevan, V.N., 2012. A new atlas of temperature and salinity  
728 for the North Indian Ocean. *J. Earth Syst. Sci.* 121, 559–593. 10.1007/  
s12040-012-0191-9.
- 730 Chaudhuri, A., Shankar, D., Aparna, S.G., Amol, P., Fernando, V.,  
Kankonkar, A., Michael, G.S., Satelkar, N.P., Khalap, S.T., Tari, A.P.,  
732 Gaonkar, M.G., Ghatkar, S., Khedekar, R.R., 2020. Observed variability  
of the West India Coastal Current on the continental slope from 2009–  
734 2018. *J. Earth Syst. Sci.* 129, 57. 10.1007/s12040-019-1322-3.
- 736 Cisewski, B., Strass, V.H., Rhein, M., Krägesky, S., 2010. Seasonal variation  
of diel vertical migration of zooplankton from ADCP backscatter time  
series data in the Lazarev Sea, Antarctica. *Deep-Sea Res. Part I Oceanogr.*  
738 *Res. Pap.* 57, 78–94. 10.1016/j.dsr.2009.10.005.
- 740 Davis, R.E., Talley, L.D., Roemmich, D., Owens, W.B., Rudnick, D.L.,  
Toole, J., Weller, R., McPhaden, M.J., Barth, J.A., 2019. 100 years of  
progress in ocean observing systems. *Meteorol. Monogr.* 59, 3–1. 10.  
742 1175/AMSMONOGRAPH-D-18-0014.1.
- 744 Deines, K.L., 1999. Backscatter estimation using broadband acoustic  
Doppler current profilers, in: Proceedings of the IEEE Sixth Working  
Conference on Current Measurement (Cat. No. 99CH36331), IEEE. pp.  
746 249–253. 10.1109/CCM.1999.755249.

- DeSousa, S.N., Dileepkumar, M., Sardessai, S., Sarma, V.V.S.S., Shirodkar,  
748 P.V., 1996. Seasonal variability in oxygen and nutrients in the central and  
eastern Arabian Sea. *Curr. Sci.* 71. [drs.nio.org/drs/handle/2264/35](http://drs.nio.org/drs/handle/2264/35).
- 750 Edvardsen, A., Slagstad, D., Tande, K.S., Jaccard, P., 2003. Assessing  
zooplankton advection in the Barents Sea using underway measurements  
752 and modelling. *Fish. Oceanogr.* 12, 61–74. [10.1046/j.1365-2419.2003.00219.x](https://doi.org/10.1046/j.1365-2419.2003.00219.x).
- 754 Flagg, C.N., Smith, S.L., 1989. On the use of the acoustic Doppler current  
profiler to measure zooplankton abundance. *Deep-Sea Res. Part A.*  
756 *Oceanogr. Res. Pap.* 36, 455–474. [10.1016/0198-0149\(89\)90047-2](https://doi.org/10.1016/0198-0149(89)90047-2).
- 758 García, H.E., Locarnini, R.A., Boyer, T.P., Antonov, J.I., Mishonov, A.V.,  
Baranova, O.K., Zweng, M.M., Reagan, J.R., Johnson, D.R., 2014. Dissolved  
oxygen, apparent oxygen utilization, and oxygen saturation. NOAA  
760 Atlas NESDIS 75 3. [data.nodc.noaa.gov/woa/WOA18/DOC/woa18\\_vol3.pdf](http://data.nodc.noaa.gov/woa/WOA18/DOC/woa18_vol3.pdf).
- 762 Greene, C.H., Wiebe, P.H., Pelkie, C., Benfield, M.C., Popp, J.M.,  
1998. Three-dimensional acoustic visualization of zooplankton patchiness.  
764 *Deep-Sea Res. Part II Top. Stud. Oceanogr.* 45, 1201–1217.  
[10.1016/S0967-0645\(98\)00034-4](https://doi.org/10.1016/S0967-0645(98)00034-4).
- 766 Greenlaw, C.F., 1979. Acoustical estimation of zooplankton populations 1.  
*Limnol. Oceanogr.* 24, 226–242. [10.4319/lo.1979.24.2.00226](https://doi.org/10.4319/lo.1979.24.2.00226).
- 768 Guerra, D., Schroeder, K., Borghini, M., Camatti, E., Pansera, M.,  
Schroeder, A., Sparnocchia, S., Chiggiato, J., 2019. Zooplankton diel  
770 vertical migration in the Corsica channel (north-western Mediterranean

- Sea) detected by a moored acoustic Doppler current profiler. *Ocean Sci.*  
772      15, 631–649. [10.5194/os-15-631-2019](https://doi.org/10.5194/os-15-631-2019).
- Hamilton, J.M., Collins, K., Prinsenberg, S.J., 2013. Links between ocean  
774 properties, ice cover, and plankton dynamics on interannual time scales  
in the Canadian Arctic Archipelago. *J. Geophys. Res. Oceans* 118, 5625–  
776 5639. [10.1002/jgrc.20382](https://doi.org/10.1002/jgrc.20382).
- Hays, G.C., 2003. A review of the adaptive significance and ecosystem  
778 consequences of zooplankton diel vertical migrations, in: *Migrations and*  
*Dispersal of Marine Organisms: Proceedings of the 37th European Ma-*  
780 *rine Biology Symposium held in Reykjavík, Iceland, 5–9 August 2002,*  
Springer. pp. 163–170. [10.1007/978-94-017-2276-6\\_18](https://doi.org/10.1007/978-94-017-2276-6_18).
- 782 Heywood, K.J., Howe, S.S., Barton, E.D., 1991. Estimation of zooplankton  
abundance from shipborne ADCP backscatter. *Deep-Sea Res. Part A.*  
784 *Oceanogr. Res. Pap.* 38, 677–691. [10.1016/0198-0149\(91\)90006-2](https://doi.org/10.1016/0198-0149(91)90006-2).
- 786 Hitchcock, G.L., Lane, P., Smith, S., Luo, J., Ortner, P.B., 2002. Zooplank-  
ton spatial distributions in coastal waters of the northern Arabian Sea,  
August, 1995. *Deep-Sea Res. Part II Top. Stud. Oceanogr.* 49, 2403–2423.  
788 [10.1016/S0967-0645\(02\)00042-5](https://doi.org/10.1016/S0967-0645(02)00042-5).
- 790 Hobbs, L., Banas, N.S., Cohen, J.H., Cottier, F.R., Berge, J., Varpe, Ø.,  
2021. A marine zooplankton community vertically structured by light  
across diel to interannual timescales. *Biol. Lett.* 17, 20200810. [10.1098/rsbl.2020.0810](https://doi.org/10.1098/rsbl.2020.0810).
- Hood, R.R., Beckley, L.E., Wiggert, J.D., 2017. Biogeochemical and ecolog-

- 794       ical impacts of boundary currents in the Indian Ocean. *Prog. Oceanogr.*  
156, 290–325. [10.1016/j.pocean.2017.04.011](https://doi.org/10.1016/j.pocean.2017.04.011).
- 796       Inoue, R., Kitamura, M., Fujiki, T., 2016. Diel vertical migration of  
zooplankton at the S1 biogeochemical mooring revealed from acous-  
798       tic backscattering strength. *J. Geophys. Res. Oceans* 121, 1031–1050.  
[10.1002/2015JC011352](https://doi.org/10.1002/2015JC011352).
- 800       Jadhav, S.J., Smitha, B., 2024. Abundance distribution pattern of zoo-  
plankton associated with the eastern Arabian Sea monsoon system as  
802       detected by underwater acoustics and net sampling. *Acoust. Aust.* , 1–  
2210. [10.1007/s40857-024-00336-w](https://doi.org/10.1007/s40857-024-00336-w).
- 804       Jiang, S., Dickey, T.D., Steinberg, D.K., Madin, L.P., 2007. Temporal vari-  
ability of zooplankton biomass from ADCP backscatter time series data  
806       at the Bermuda Testbed Mooring site. *Deep-Sea Res. Part I Oceanogr.*  
Res. Pap. 54, 608–636. [10.1016/j.dsr.2006.12.011](https://doi.org/10.1016/j.dsr.2006.12.011).
- 808       Jyothibabu, R., Madhu, N.V., Habeebrehman, H., Jayalakshmy, K.V., Nair,  
K.K.C., Achuthankutty, C.T., 2010. Re-evaluation of ‘paradox of meso-  
810       zooplankton’ in the eastern Arabian Sea based on ship and satellite obser-  
vations. *J. Mar. Syst.* 81, 235–251. [10.1016/j.jmarsys.2009.12.019](https://doi.org/10.1016/j.jmarsys.2009.12.019).
- 812       Kang, M., Oh, S., Oh, W., Kang, D.J., Nam, S., Lee, K., 2024. Acoustic  
characterization of fish and macroplankton communities in the Seychelles-  
814       Chagos Thermocline Ridge of the southwest Indian Ocean. *Deep-Sea*  
Res. Part II Top. Stud. Oceanogr. 213, 105356. [10.1016/j.dsr2.2023.105356](https://doi.org/10.1016/j.dsr2.2023.105356).
- 816       Keerthi, M.G., Lengaigne, M., Lévy, M., Vialard, J., Parvathi, V.,

- 818 de Boyer Montégut, C., Ethé, C., Aumont, O., Suresh, I., Akhil, V.P.,  
Muraleedharan, P.M., 2017. Physical control of interannual variations of  
820 the winter chlorophyll bloom in the northern Arabian Sea. *Biogeosci.* 14,  
3615–3632. [10.5194/bg-14-3615-2017](https://doi.org/10.5194/bg-14-3615-2017).
- 822 Khandagale, P.A., Mhatre, V.D., Thomas, S., 2022. Seasonal and spatial  
variability of zooplankton diversity in north eastern Arabian Sea along  
824 the Maharashtra coast. *J. Mar. Biol. Assoc. India* 64, 25–32. [mbai.org.in/php/journaldload.php?id=2618&bkid=128](http://mbai.org.in/php/journaldload.php?id=2618&bkid=128).
- 826 Kumar, S.P., Narvekar, J., 2005. Seasonal variability of the mixed layer  
in the central Arabian Sea and its implication on nutrients and primary  
828 productivity. *Deep-Sea Res. Part II Top. Stud. Oceanogr.* 52, 1848–1861.  
[10.1016/j.dsr2.2005.06.002](https://doi.org/10.1016/j.dsr2.2005.06.002). biogeochemical Processes in the North-  
830 ern Indian Ocean.
- 832 Lawson, G.L., Wiebe, P.H., Ashjian, C.J., Gallager, S.M., Davis, C.S., Warren,  
J.D., 2004. Acoustically-inferred zooplankton distribution in relation  
to hydrography west of the Antarctic Peninsula. *Deep-Sea Res. Part II  
Top. Stud. Oceanogr.* 51, 2041–2072. [10.1016/j.dsr2.2004.07.022](https://doi.org/10.1016/j.dsr2.2004.07.022).
- 834 Lévy, M., Shankar, D., André, J.M., Shenoi, S.S.C., Durand, F.,  
836 de Boyer Montégut, C., 2007. Basin-wide seasonal evolution of the  
Indian Ocean's phytoplankton blooms. *J. Geophys. Res. Oceans* 112.  
[10.1029/2007JC004090](https://doi.org/10.1029/2007JC004090).
- 840 Li, M., Gargett, A., Denman, K., 2000. What determines seasonal and  
interannual variability of phytoplankton and zooplankton in strongly es-  
842 tuarine systems? *Estuar. Coast. Shelf Sci.* 50, 467–488. [10.1006/ecss.2000.0593](https://doi.org/10.1006/ecss.2000.0593).

- Liu, Y., Guo, J., Xue, Y., Sangmanee, C., Wang, H., Zhao, C., Khokiattiwong, S., Yu, W., 2022. Seasonal variation in diel vertical migration of zooplankton and micronekton in the Andaman Sea observed by a moored ADCP. Deep-Sea Res. Part I Oceanogr. Res. Pap. 179, 103663. 10.1016/j.dsr.2021.103663.
- Madhupratap, M., Gopalakrishnan, T.C., Haridas, P., Nair, K.K.C., Aravindakshan, P.N., Padmavati, G., Paul, S., 1996a. Lack of seasonal and geographic variation in mesozooplankton biomass in the Arabian Sea and its structure in the mixed layer. Curr. Sci. 71, 863–868. drs.nio.org/drs/handle/2264/2154.
- Madhupratap, M., Haridas, P., Ramaiah, N., Achuthankutty, C.T., 1992. Zooplankton of the southwest coast of India: abundance, composition, temporal and spatial variability in 1987. Oceanogr. Indian Ocean .
- Madhupratap, M., Kumar, S.P., Bhattathiri, P.M.A., Kumar, M.D., Raghukumar, S., Nair, K.K.C., Ramaiah, N., 1996b. Mechanism of the biological response to winter cooling in the northeastern Arabian Sea. Nature 384, 549–552. 10.1038/384549a0.
- McCreary, J.P., Kohler, K.E., Hood, R.R., Olson, D.B., 1996. A four-component ecosystem model of biological activity in the Arabian Sea. Prog. Oceanogr. 37, 193–240. 10.1016/S0079-6611(96)00005-5.
- McCreary, J.P., Kundu, P.K., Molinari, R.L., 1993. A numerical investigation of dynamics, thermodynamics and mixed-layer processes in the Indian Ocean. Prog. Oceanogr. 31, 181–244. 10.1016/0079-6611(93)90002-U.
- McCreary, J.P., Murtugudde, R., Vialard, J., Vinayachandran, P.N., Wig-

- gert, J.D., Hood, R.R., Shankar, D., Shetye, S.R., 2009. Biophysical processes in the Indian Ocean. *Indian Ocean Biogeochem. Processes Ecol. Variab.* 185, 9–32. [10.1029/2008GM000768](https://doi.org/10.1029/2008GM000768).
- Mooley, D.A., Parthasarathy, B., 1984. Fluctuations in all-India summer monsoon rainfall during 1871–1978. *Clim. Change* 6, 287–301. [10.1007/BF00142477](https://doi.org/10.1007/BF00142477).
- Mukherjee, A., Shankar, D., Fernando, V., Amol, P., Aparna, S.G., Fernandes, R., Michael, G.S., Khalap, S.T., Satelkar, N.P., Agarvadekar, Y., Gaonkar, M.G., Tari, A.P., Kankonkar, A., Vernekar, S., 2014. Observed seasonal and intraseasonal variability of the East India Coastal Current on the continental slope. *J. Earth Syst. Sci.* 123, 1197–1232. [10.1007/s12040-014-0471-7](https://doi.org/10.1007/s12040-014-0471-7).
- Mukhopadhyay, S., Shankar, D., Aparna, S.G., Mukherjee, A., 2017. Observations of the sub-inertial, near-surface East India Coastal Current. *Cont. Shelf Res.* 148, 159–177. [10.1016/j.csr.2017.08.020](https://doi.org/10.1016/j.csr.2017.08.020).
- Mukhopadhyay, S., Shankar, D., Aparna, S.G., Mukherjee, A., Fernando, V., Kankonkar, A., Khalap, S., Satelkar, N.P., Gaonkar, M.G., Tari, A.P., Khedkar, R.R., Ghatkar, S., 2020. Observed variability of the East India Coastal Current on the continental slope during 2009–2018. *J. Earth Syst. Sci.* 129, 1–22. [10.1007/s12040-020-1346-8](https://doi.org/10.1007/s12040-020-1346-8).
- Nair, K.K.C., Madhupratap, M., Gopalakrishnan, T.C., Haridas, P., Gauns, M., 1999. The Arabian Sea: physical environment, zooplankton and myctophid abundance. *Indian J. Mar. Sci.* 28, 138–145. [nopr.niscpr.res.in/handle/123456789/25690](https://nopr.niscpr.res.in/handle/123456789/25690).

- Nair, P.V., 1970. Primary productivity in the Indian seas. CMFRI Bulletin  
892 22, 1–63. [eprints.cmfri.org.in/id/eprint/610](http://eprints.cmfri.org.in/id/eprint/610).
- Naqvi, S.W.A., Narvekar, P.V., Desa, E., 2006. Coastal biogeochemical pro-  
894 cesses in the north Indian Ocean. Coastal segment (14,S–W), in: Robinson,  
A.R., Brink, K.H. (Eds.), *The Sea*. John Wiley and Sons, Inc. vol-  
896 ume 14. chapter 19, pp. 723–781.
- Naqvi, S.W.A., Noronha, R.J., Somasundar, K., Gupta, R.S., 1990. Sea-  
898 sonal changes in the denitrification regime of the Arabian Sea. Deep-Sea  
Research 37, 593–611. [10.1016/0198-0149\(90\)90092-A](https://doi.org/10.1016/0198-0149(90)90092-A).
- 900 Nie, L., Li, J., Wu, H., Zhang, W., Tian, Y., Liu, Y., Sun, P., Ye, Z., Ma, S.,  
Gao, Q., 2023. The influence of ocean processes on fine-scale changes in  
902 the Yellow Sea cold water mass boundary area structure based on acoustic  
observations. Rem. Sens. 15, 4272. [10.3390/rs15174272](https://doi.org/10.3390/rs15174272).
- 904 Ohman, M.D., Hirche, H.J., 2001. Density-dependent mortality in an  
oceanic copepod population. Nature 412, 638–641. [10.1038/35088068](https://doi.org/10.1038/35088068).
- 906 Piontkovski, S.A., Williams, R., Melnik, T.A., 1995. Spatial heterogene-  
ity, biomass and size structure of plankton of the Indian Ocean: some  
908 general trends. Mar. Ecol. Prog. Ser. , 219–227[www.jstor.org/stable/44634833](http://www.jstor.org/stable/44634833).
- 910 Potiris, E., Frangoulis, C., Kalampokis, A., Ntoumas, M., Pettas, M., Peti-  
hakis, G., Zervakis, V., 2018. Acoustic doppler current profiler observa-  
912 tions of migration patterns of zooplankton in the Cretan Sea. Ocean Sci.  
14, 783–800. [10.5194/os-14-783-2018](https://doi.org/10.5194/os-14-783-2018).

- 914 Prasad, T., Bahulayan, N., 1996. Mixed layer depth and thermocline climatology of the Arabian Sea and western equatorial Indian Ocean. Indian J.  
916 Mar. Sci. 25, 189–194. [nopr.niscpr.res.in/handle/123456789/37119](http://nopr.niscpr.res.in/handle/123456789/37119).
- 918 Qasim, S.Z., 1977. Biological productivity of the Indian Ocean. Indian J.  
Mar. Sci. 6, 122–137. [nopr.niscpr.res.in/handle/123456789/39365](http://nopr.niscpr.res.in/handle/123456789/39365).
- 920 Quéré, C.L., Andrew, R.M., Canadell, J.G., Sitch, S., Korsbakken, J.I.,  
Peters, G.P., Manning, A.C., Boden, T.A., Tans, P.P., Houghton, R.A.,  
2016. Global carbon budget 2016. Earth Syst. Sci. Data 8, 605–649.  
922 [10.5194/essd-8-605-2016](https://doi.org/10.5194/essd-8-605-2016).
- 924 Ramamurthy, S., 1965. Studies on the plankton of the North Kanara coast  
in relation to the pelagic fishery. J. Mar. Biol. Assoc. India 7, 127–149.  
[eprints.cmfri.org.in/id/eprint/894](http://eprints.cmfri.org.in/id/eprint/894).
- 926 Rehim, M., Imran, M., 2012. Dynamical analysis of a delay model of  
phytoplankton-zooplankton interaction. Appl. Math. Model. 36, 638–647.  
928 [10.1016/j.apm.2011.07.018](https://doi.org/10.1016/j.apm.2011.07.018).
- 930 Rippeth, T.P., Simpson, J.H., 1998. Diurnal signals in vertical motions  
on the Hebridean shelf. Limnol. Oceanogr. 43, 1690–1696. [10.4319/lo.1998.43.7.1690](https://doi.org/10.4319/lo.1998.43.7.1690).
- 932 Rochford, D., 1964. Salinity maxima in the upper 1000 metres of the north  
Indian Ocean. Marine and Freshwater Research 15, 1–24. [10.1071/MF9640001](https://doi.org/10.1071/MF9640001).
- 934 Ryther, J.H., Hall, J.R., Pease, A.K., Bakun, A., Jones, M.M., 1966.  
Primary organic production in relation to the chemistry and hydrogra-

- phy of the western Indian Ocean. Limnol. and Oceanogr. 11, 371–380.  
938 10.4319/lo.1966.11.3.0371.
- Schmidt, H., Czeschel, R., Visbeck, M., 2020. Seasonal variability of the  
940 Arabian Sea intermediate circulation and its impact on seasonal changes  
of the upper oxygen minimum zone. Ocean Sci. 16, 1459–1474. 10.5194/  
942 os-16-1459-2020.
- Shankar, D., Remya, R., Anil, A.C., Vijith, V., 2019. Role of physical  
944 processes in determining the nature of fisheries in the eastern Arabian  
Sea. Prog. Oceanogr. 172, 124–158. 10.1016/j.pocean.2018.11.006.
- 946 Shankar, D., Remya, R., Vinayachandran, P.N., Chatterjee, A., Behera, A.,  
2016. Inhibition of mixed-layer deepening during winter in the north-  
948 eastern Arabian Sea by the West India Coastal Current. Clim. Dyn. 47,  
1049–1072. 10.1007/s00382-015-2888-3.
- 950 Shankar, D., Shenoi, S.S.C., Nayak, R.K., Vinayachandran, P.N., Nam-  
poothiri, G., Almeida, A.M., Michael, G.S., Kumar, M.R.R., Sun-  
952 dar, D., Sreejith, O.P., 2005. Hydrography of the eastern Arabian  
Sea during summer monsoon 2002. J. Earth Syst. Sci. 114, 459–474.  
954 10.1007/BF02702023.
- Shankar, D., Shetye, S.R., 1997. On the dynamics of the Lakshadweep high  
956 and low in the southeastern Arabian Sea. J. Geophys. Res. Oceans 102,  
12551–12562. 10.1029/97JC00465.
- 958 Shankar, D., Vinayachandran, P., Unnikrishnan, A., 2002. The monsoon  
currents in the north Indian Ocean. Prog. in ocean. 52, 63–120. 10.1016/  
960 S0079-6611(02)00024-1.

- Shenoi, S.S.C., Shankar, D., Michael, G.S., Kurian, J., Varma, K.K., Kumar,  
962 M.R.R., Almeida, A.M., Unnikrishnan, A.S., Fernandes, W., Barreto, N.,  
Gnanaseelan, C., Mathew, R., Praju, K.V., Mahale, V., 2005. Hydrogra-  
964 phy and water masses in the southeastern Arabian Sea during March–June  
2003. *J. Earth Syst. Sci.* 114, 475–491. [10.1007/BF02702024](https://doi.org/10.1007/BF02702024).
- 966 Shenoi, S.S.C., Shankar, D., Shetye, S.R., 2004. Remote forcing annihilates  
barrier layer in southeastern Arabian Sea. *Geophys. Res. Lett.* [10.1029/2003GL019270](https://doi.org/10.1029/2003GL019270).
- 970 Shetye, S.R., Gouveia, A.D., Shenoi, S.S.C., 1992. Does winter cool-  
ing lead to the subsurface salinity minimum off Saurashtra, India?  
972 *Oceanogr. Indian Ocean*, 617–625 [drs.nio.org/drss/bitstream/2264/3139/2/Oceanogr\\_Indian\\_Ocean\\_1992\\_617.pdf](https://dris.nio.org/drss/bitstream/2264/3139/2/Oceanogr_Indian_Ocean_1992_617.pdf).
- 974 Shetye, S.R., Gouveia, A.D., Shenoi, S.S.C., Michael, G.S., Sundar, D.,  
Almeida, A.M., Santanam, K., 1991. The coastal current off western  
India during the northeast monsoon. *Deep-Sea Res. Part A. Oceanogr.*  
976 *Res. Pap.* 38, 1517–1529. [10.1016/0198-0149\(91\)90087-V](https://doi.org/10.1016/0198-0149(91)90087-V).
- 978 Shetye, S.R., Gouveia, A.D., Shenoi, S.S.C., Sundar, D., Michael, G.S.,  
Almeida, A., Santanam, K., 1990. Hydrography and circulation off the  
west coast of India during the southwest monsoon 1987. *J. Mar. Res.* 48,  
980 359–378.
- 982 Shi, W., Wang, M., 2022. Phytoplankton biomass dynamics in the Arabian  
Sea from VIIRS observations. *J. Mar. Syst.* 227, 103670. [10.1016/j.jmarsys.2021.103670](https://doi.org/10.1016/j.jmarsys.2021.103670).
- 984 Smeti, H., Pagano, M., Menkes, C., Dhaussy, A.L., Hunt, B.P.V., Allain, V.,

- 986 Rodier, M., De Boissieu, F., Kestenare, E., Sammari, C., 2015. Spatial  
and temporal variability of zooplankton off New Caledonia (Southwestern  
Pacific) from acoustics and net measurements. *J. Geophys. Res. Oceans*  
988 120, 2676–2700. [10.1002/2014JC010441](https://doi.org/10.1002/2014JC010441).
- 990 Smith, S.L., Madhupratap, M., 2005. Mesozooplankton of the Arabian  
Sea: patterns influenced by seasons, upwelling, and oxygen concentrations. *Prog. Oceanogr.* 65, 214–239. [10.1016/j.pocean.2005.03.007](https://doi.org/10.1016/j.pocean.2005.03.007).
- 992 994 Sreenivas, P., Patnaik, K.V.K.R.K., Prasad, K.V.S.R., 2008. Monthly vari-  
ability of mixed layer over Arabian Sea using ARGO data. *Mar. Geod.*  
31, 17–38. [10.1080/01490410701812311](https://doi.org/10.1080/01490410701812311).
- 996 Subrahmanyam, R., 1959. Studies on the phytoplankton of the west coast of  
India: Part II. Physical and chemical factors influencing the production  
of phytoplankton, with remarks on the cycle of nutrients and on the re-  
998 lationship of the phosphate-content to fish landings, in: *Proc. Ind. Acad.  
Sci.*, Springer. pp. 189–252. [10.1007/BF03051925](https://doi.org/10.1007/BF03051925).
- 1000 1002 Subrahmanyam, R., Sarma, A.H., 1960. Studies on the phytoplankton of the  
west coast of India. Part III. Seasonal variation of the phytoplankters and  
environmental factors. *Indian J. Fish.* 7, 307–336. [eprints.cmfri.org.in/1899/](https://eprints.cmfri.org.in/1899/).
- 1004 Ursella, L., Cardin, V., Batistić, M., Garić, R., Gačić, M., 2018. Evidence of  
zooplankton vertical migration from continuous Southern Adriatic buoy  
1006 current-meter records. *Prog. Oceanogr.* 167, 78–96. [10.1016/j.pocean.2018.07.004](https://doi.org/10.1016/j.pocean.2018.07.004).
- 1008 Ursella, L., Pensieri, S., Pallàs-Sanz, E., Herzka, S.Z., Bozzano, R., Tenreiro,

- M., Cardin, V., Candela, J., Sheinbaum, J., 2021. Diel, lunar and seasonal  
1010 vertical migration in the deep western Gulf of Mexico evidenced from  
a long-term data series of acoustic backscatter. *Prog. Oceanogr.* 195,  
1012 102562. [10.1016/j.pocean.2021.102562](https://doi.org/10.1016/j.pocean.2021.102562).
- Vijith, V., Shetye, S.R., Gouveia, A.D., Shenoi, S.S.C., Michael, G.S., Sun-  
1014 dar, D., 2022. Circulation in the region of the West India Coastal Current  
in March 1994 hydrographic and altimeter data. *J. Earth Syst. Sci.* 131,  
1016 16. [10.1007/s12040-021-01761-5](https://doi.org/10.1007/s12040-021-01761-5).
- Vijith, V., Vinayachandran, P.N., Thushara, V., Amol, P., Shankar, D.,  
1018 Anil, A.C., 2016. Consequences of inhibition of mixed-layer deepening  
by the West India Coastal Current for winter phytoplankton bloom in  
1020 the northeastern Arabian Sea. *J. Geophys. Res. Oceans* 121, 6583–6603.  
[10.1002/2016JC012004](https://doi.org/10.1002/2016JC012004).
- Wiebe, P.H., Greene, C.H., Stanton, T.K., Burczynski, J., 1990. Sound  
1022 scattering by live zooplankton and micronekton: empirical studies with  
1024 a dual-beam acoustical system. *The Journal of the Acoustical Society of  
America* 88, 2346–2360. [10.1121/1.400077](https://doi.org/10.1121/1.400077).
- Winder, M., Schindler, D.E., 2004. Climatic effects on the phenology of lake  
1026 processes. *Global Change Biol.* 10, 1844–1856. [10.1111/j.1365-2486.2004.00849.x](https://doi.org/10.1111/j.1365-2486.2004.00849.x).
- Wishner, K.F., Gowing, M.M., Gelfman, C., 1998. Mesozooplankton  
1030 biomass in the upper 1000 m in the Arabian Sea: overall seasonal and  
geographic patterns, and relationship to oxygen gradients. *Deep-Sea Res.*  
1032 Part II Top. Stud. Oceanogr. 45, 2405–2432. [10.1016/S0967-0645\(98\)00078-2](https://doi.org/10.1016/S0967-0645(98)00078-2).

1034 Wyrtki, K., Bennett, E.B., Rochford, D.J., Expedition, I.I.O., (U.S.),  
N.S.F., of Hawaii (Honolulu), U., 1971. Oceanographic atlas of the  
1036 International Indian Ocean Expedition. National Science Foundation.  
[//cir.nii.ac.jp/crid/1130000796355741312](http://cir.nii.ac.jp/crid/1130000796355741312).





165–168	G7	–	5 Jan 23	1935	50 – 25 , 75 – 50 , 100 – 75 , 150 – 100
169–172	J4	–	4 Jan 23	1134	50 – 25 , 75 – 50 , 100 – 75 , 150 – 100
173–176	M6	–	2 Jan 23	1950	50 – 25 , 75 – 50 , 100 – 75 , 150 – 100
177–180	U4	–	6 Jan 23	1538	50 – 25 , 75 – 50 , 100 – 75 , 150 – 100
181–184	K5	–	8 Jan 23	1156	50 – 25 , 75 – 50 , 100 – 75 , 150 – 100

---

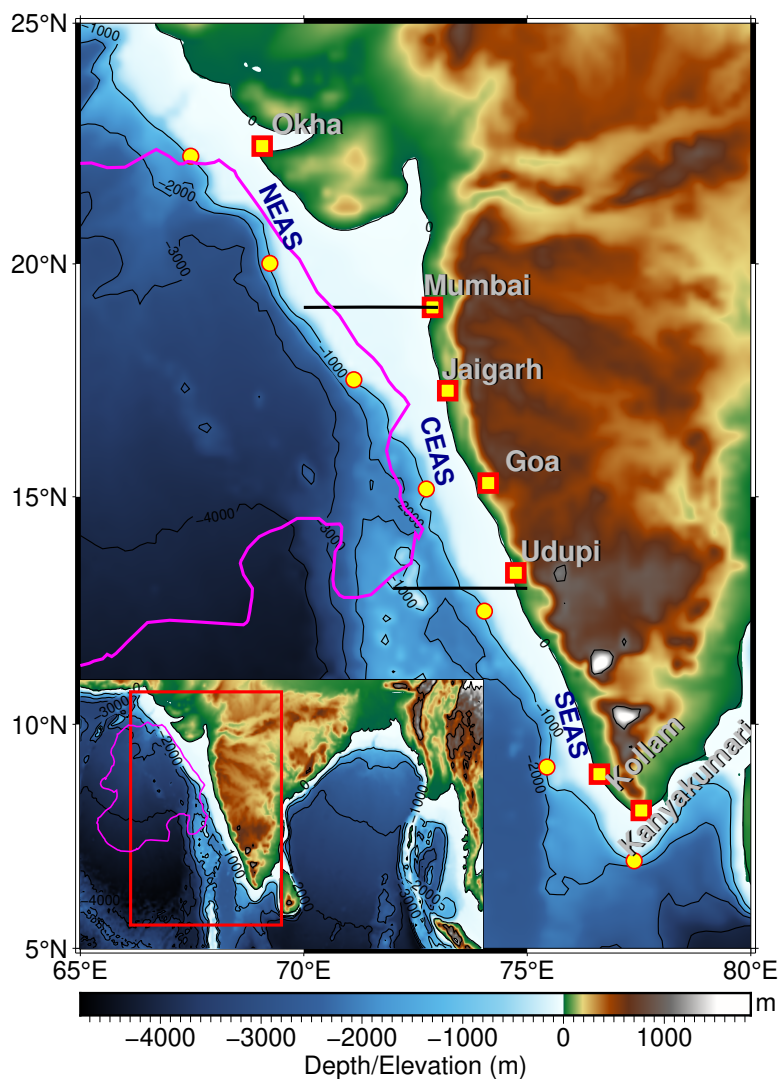


**Figure 1:** Map showing the region of interest in the eastern Arabian Sea. Slope moorings are deployed at  $\sim 1000$  m depth, indicated by bathymetry contours. Shelf width increases poleward along the coast. Mooring sites off Okha and Mumbai are in the NEAS, Jaigarh and Goa in the CEAS, and Kollam and Kanyakumari in the SEAS. Udupi lies north of transition line between CEAS and SEAS. The OMZ is marked by the area enclosed within magenta contours, following A22 (Naqvi et al., 1990; Smith and Madhupratap, 2005).

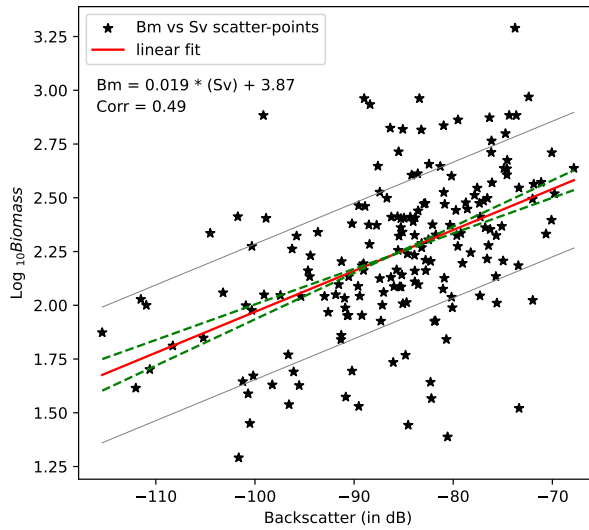


**Figure 2:** Linear regression of biomass (log<sub>10</sub> scale) and backscattering strength (in dB) is shown. The fit lies within the error bounds of Aparna et al. (2022), which used 67 data points; the updated dataset includes 184 points with newly appended volumetric zooplankton samples. The regression equation is  $y = 0.019x + 3.87$ , with a correlation coefficient of 0.49. Dashed green lines indicate the error bounds of the slope and intercept. This range leads to an estimated uncertainty of  $\sim 14 \text{ mg m}^{-3}$  in biomass. The standard deviation of log<sub>10</sub>(Biomass) is  $\pm 0.49$ , corresponding to a backscatter range of 48.58 dB, encompassing the full observed range and supporting the robustness of biomass dependence on ADCP-derived backscatter.

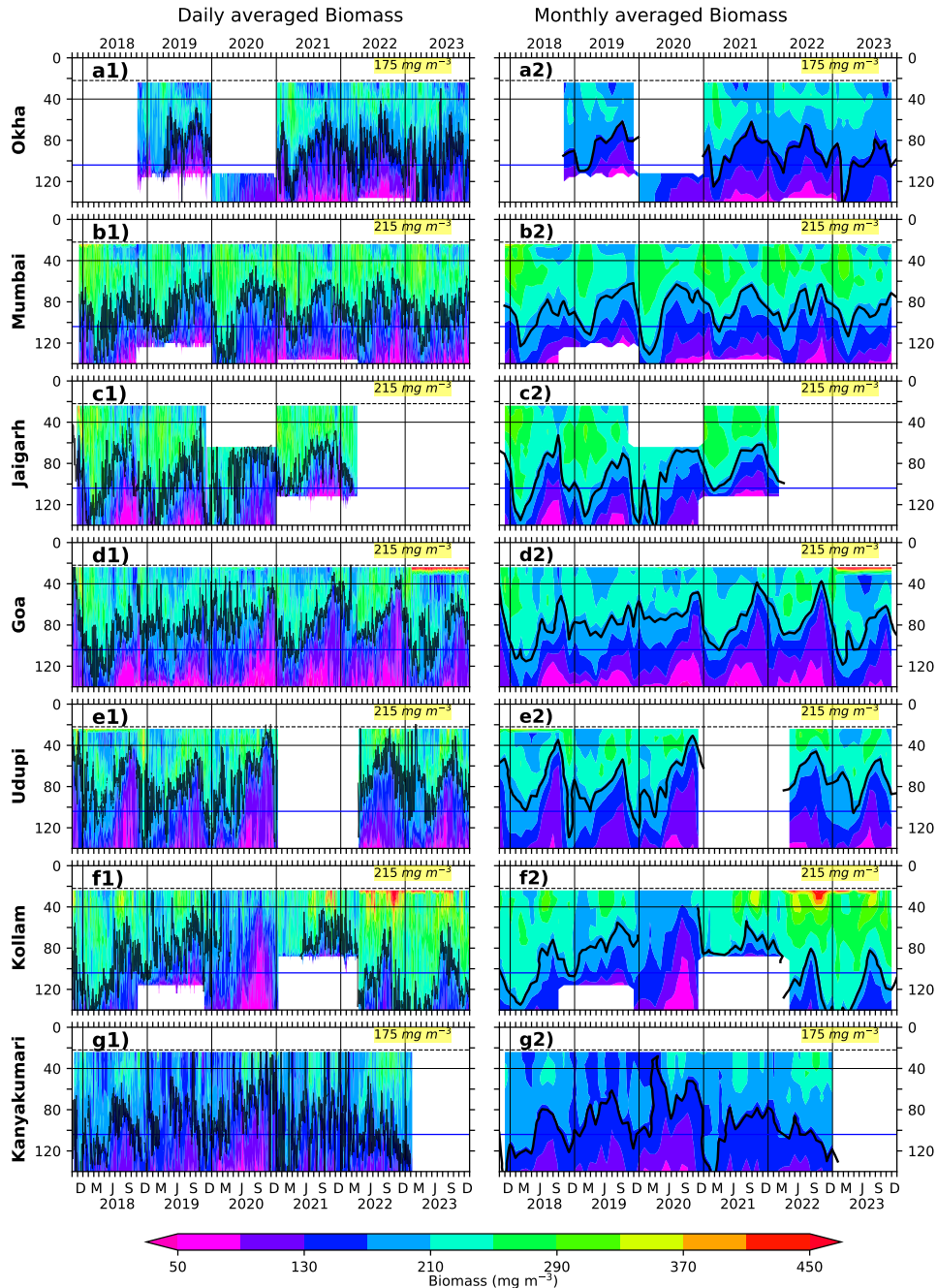


**Figure 3:** Daily and monthly averaged biomass for EAS moorings arranged from north (top) to south (bottom). Black contours mark  $175 \text{ mg m}^{-3}$  biomass for Okha and Kanyakumari, and  $215 \text{ mg m}^{-3}$  for the remaining locations. These thresholds are location-specific and best capture seasonality based on local physico-chemical conditions. The top 10% of data is excluded due to echo noise. The dashed line at 22 m marks the top edge of the first bin (i.e., 24 m). Vertical black lines separate years, while horizontal black and blue lines indicate 40 m and 104 m depths, respectively. Off Kollam in 2020, no consistent biomass contour is shown due to strong interannual variability.

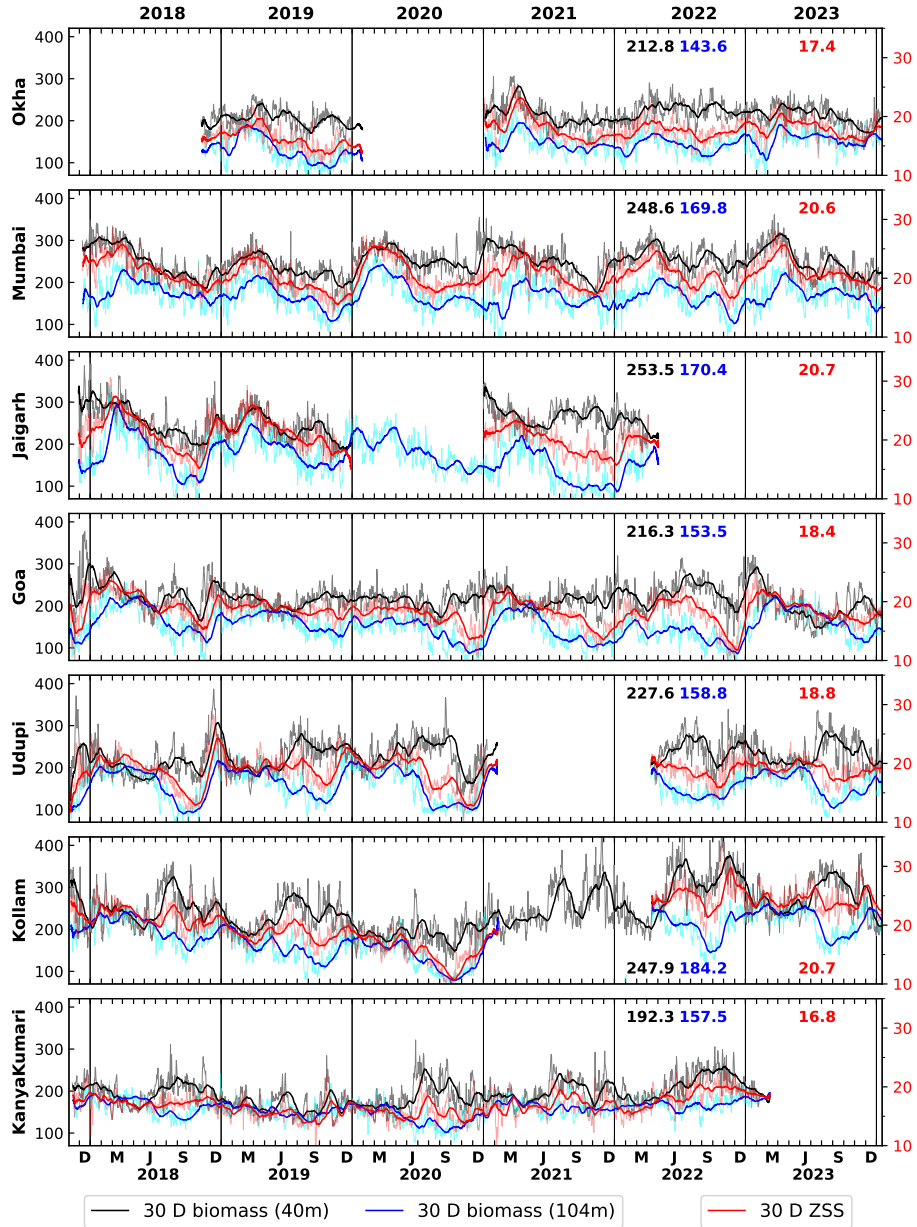


**Figure 4:** Biomass at 40 m (grey, black) and 104 m (cyan, blue), along with ZSS (pink, red; integrated over 24–120 m), is shown with lighter shades representing daily values and darker shades indicating 30-day rolling averages. Mean biomass at 40 m, 104 m, and mean ZSS are noted in the top-right corner in corresponding colors. Spikes (bursts) in biomass at 40 m appear in the daily (rolling mean) data, typically lasting a few days (or several days to weeks), e.g., during isolated days in June 2020 (or throughout June–July 2020) off the SEAS. Similar features are observed at all locations at both depths, though with varying magnitudes.

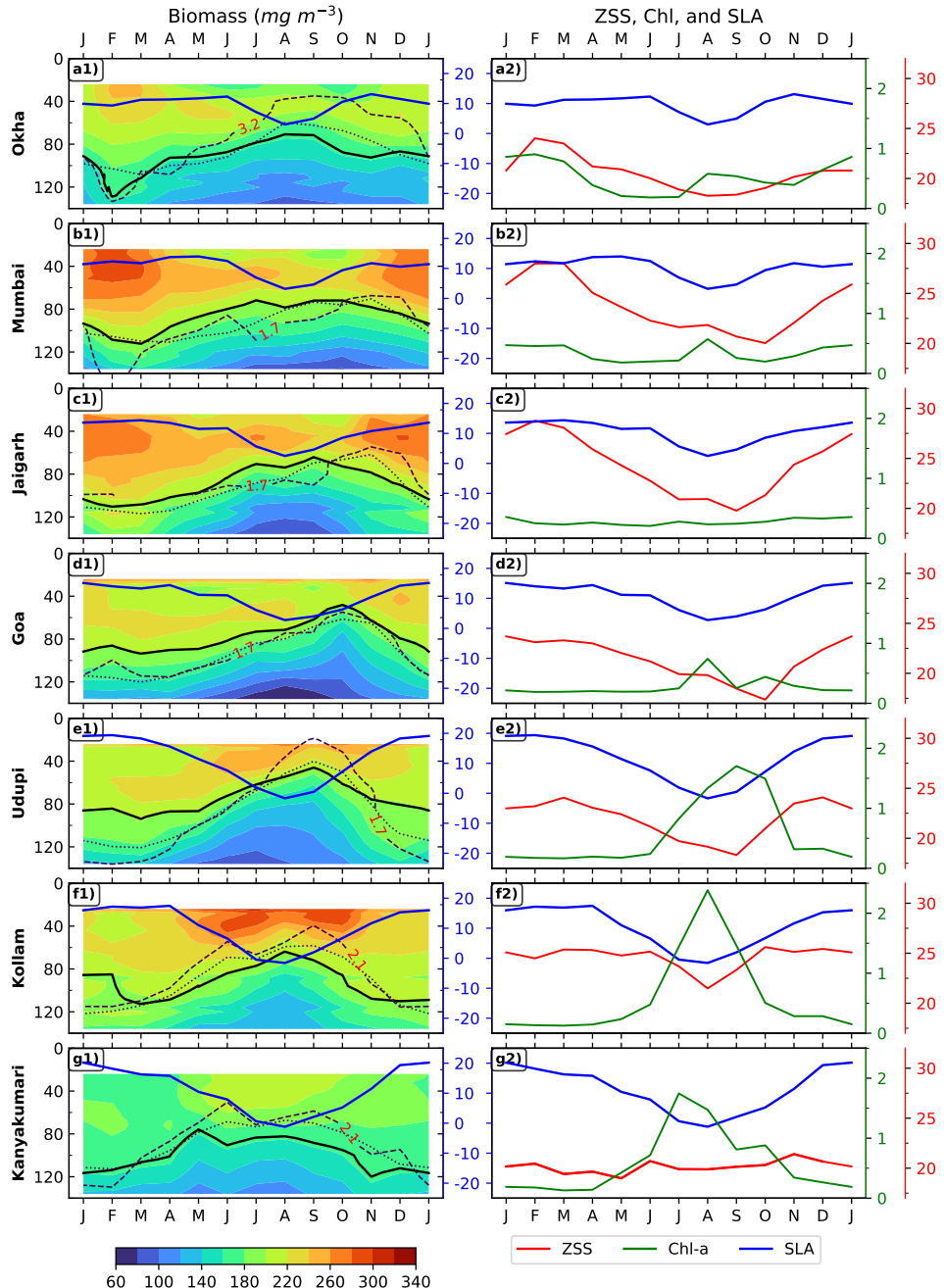


**Figure 5:** Monthly climatology of zooplankton biomass is shown in the left panels for seven locations. D175 and D215 are shown as solid lines; the dashed line indicates the depth of the  $23^{\circ}\text{C}$  isotherm, and oxygen contours are shown as dotted lines and labeled for each mooring. The right panels display the ZSS (biomass integrated over 24–140 m) and chl-*a* climatology for the corresponding locations, overlaid onto sea level anomaly (SLA).

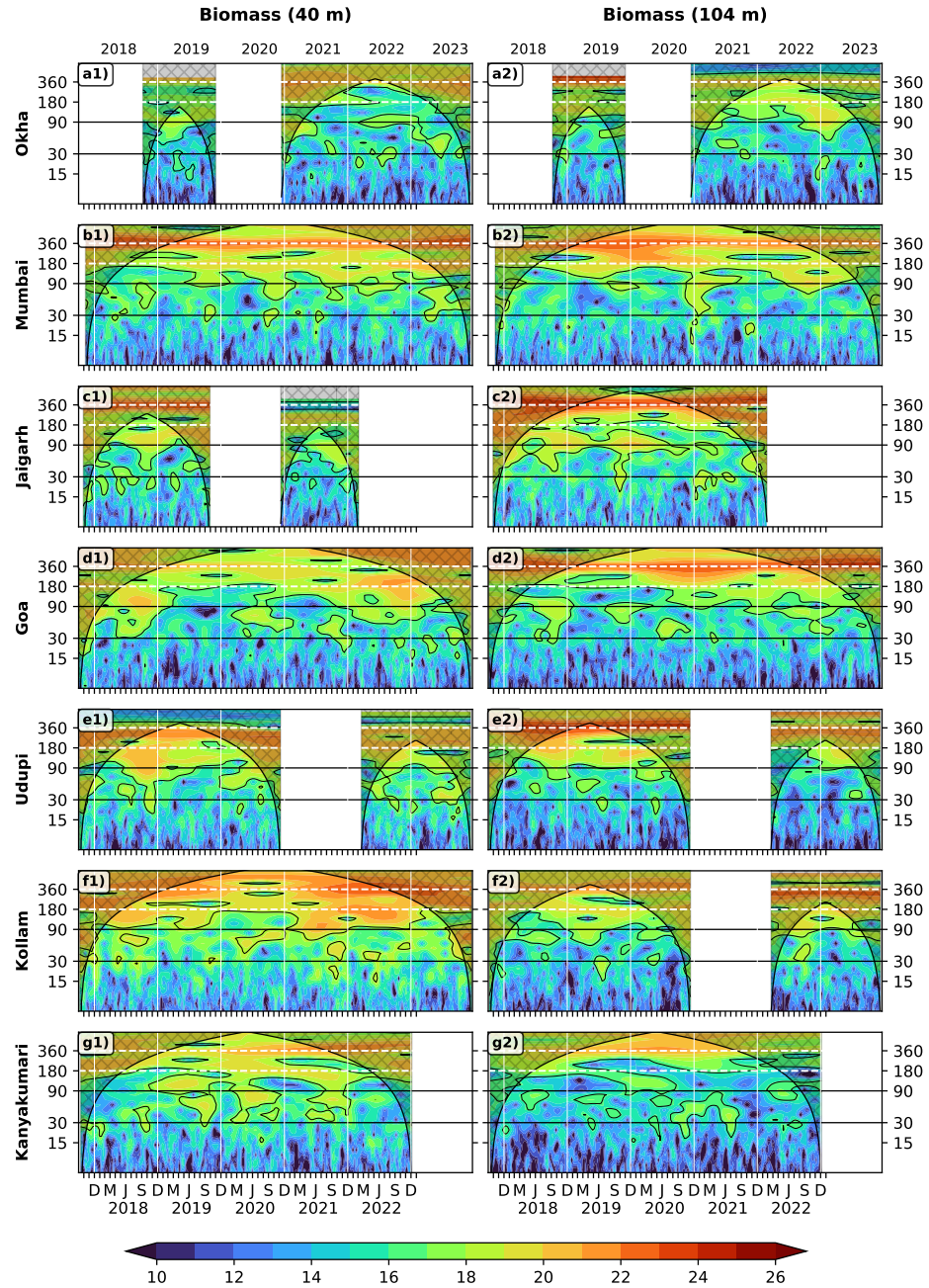


**Figure 6:** Wavelet power spectra (Morlet) of zooplankton biomass at 40 m (left panel) and 104 m (right panel), with time on the x-axis and period (in days) on the y-axis. Power is shown on a  $\log_2$  scale. The 95% significance level is outlined by black contours, and the cross-hatched region indicates the cone of influence. Horizontal dashed white and solid black lines mark the annual/semi-annual and intraseasonal bands, respectively. Vertical white lines separate years.

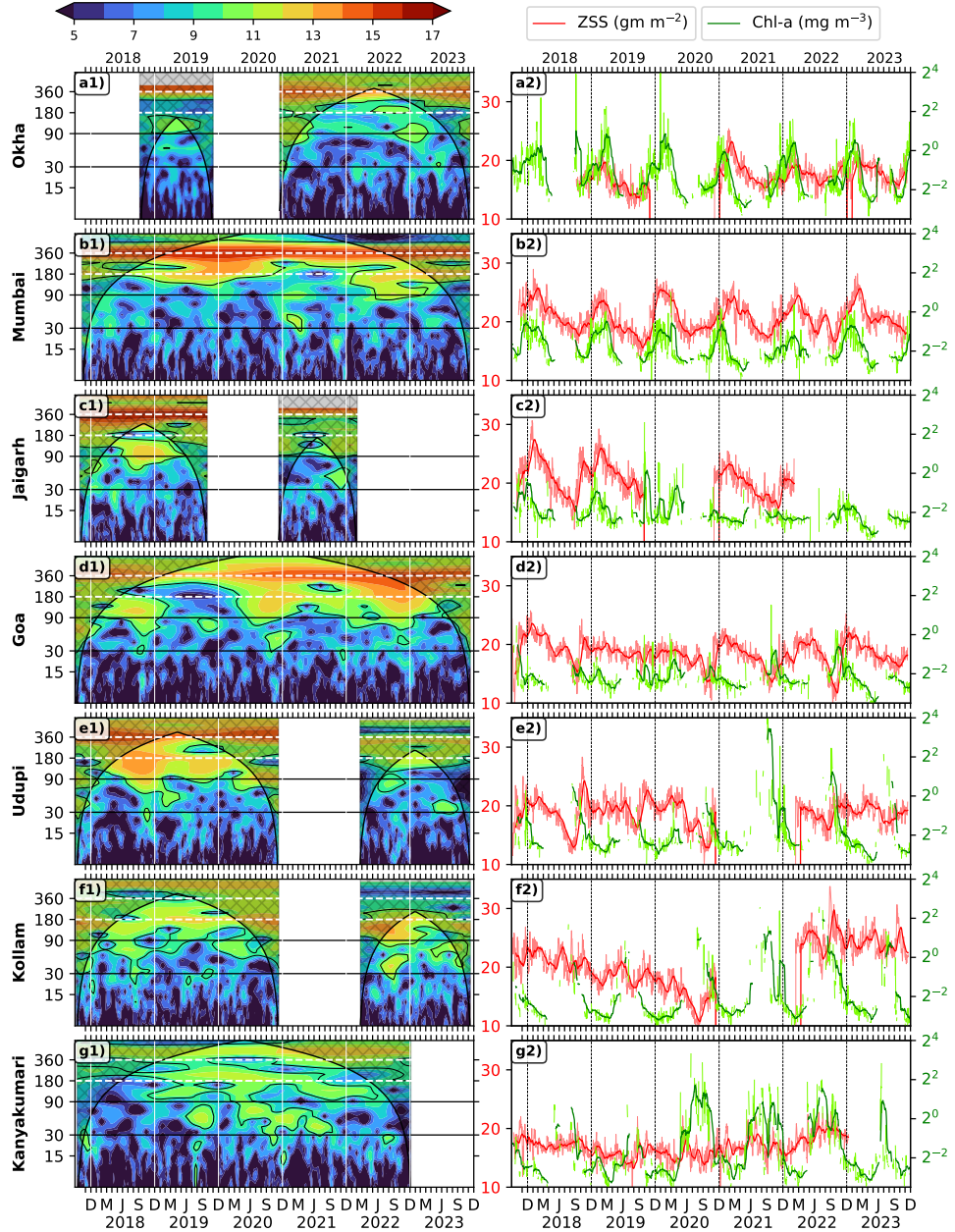


**Figure 7:** Wavelet power spectra of ZSS are shown in the left panel, with time on the x-axis and period (in days) on the y-axis. Power is displayed on a log<sub>2</sub> scale, and regions exceeding the 95% significance level are outlined in black. Vertical white lines separate years. The right panel shows the ZSS (24–120 m biomass integral) time series, with the 30-day rolling mean (red) overlaid on daily values (pink). Similarly, the 30-day rolling mean of chl-a (solid green) is plotted over its daily values (light green). Rolling means for chl-a and ZSS are computed only when at least 10 and 25 valid data points, respectively, are available within the 30-day window. The higher power off Mumbai and Goa in annual band coincides with the annual band at 40 and 104 m Fig. 6.

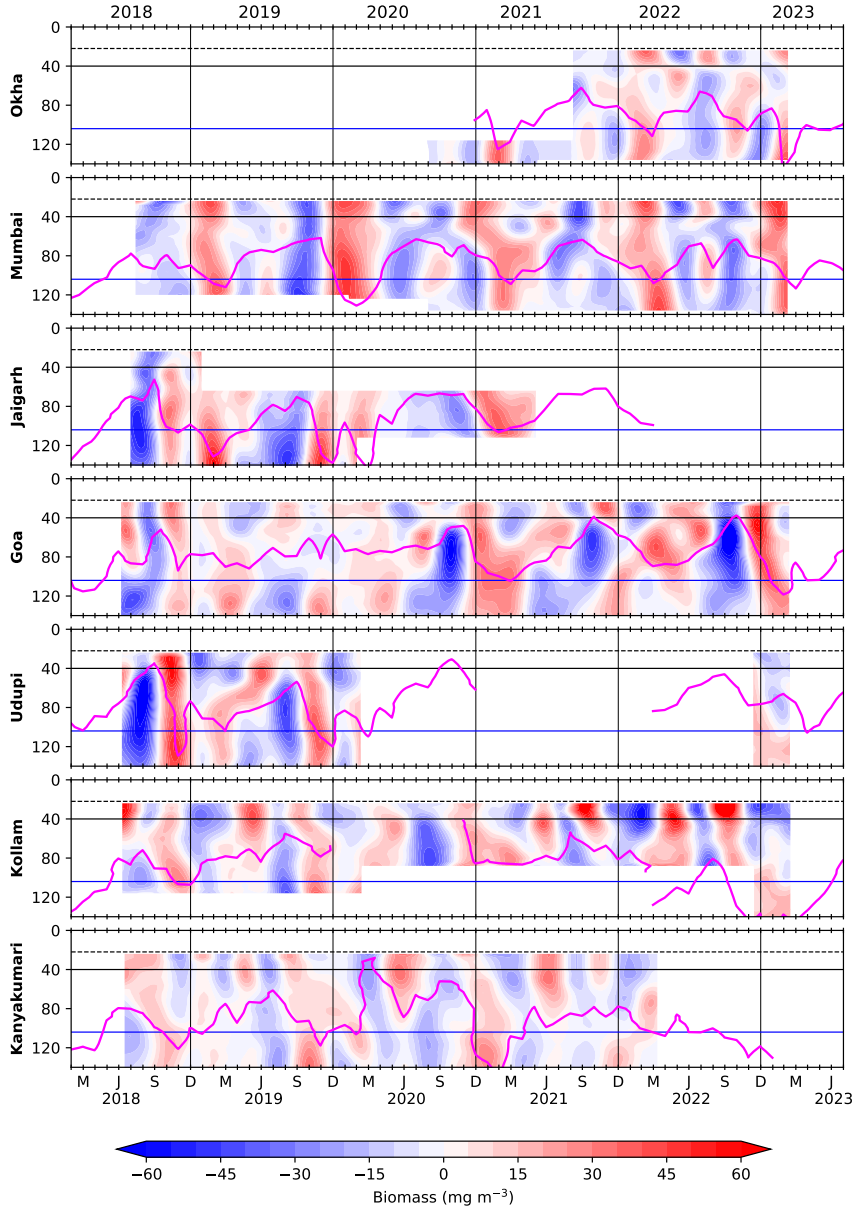


**Figure 8:** Biomass variation in the combined seasonal band (100–400 days). The seasonal cycle includes: (1) annual variation driven by upwelling (downwelling) during the summer (winter) monsoon, and (2) intra-annual variation due to seasonal asymmetry. Horizontal black and blue lines indicate 40 m and 104 m depths, respectively; vertical grey lines separate years. The dashed line at 22 m marks the upper edge of the first bin (i.e., 24 m). Solid magenta curves denote D215 (D175 off Okha and Kanyakumari), derived from monthly biomass data.

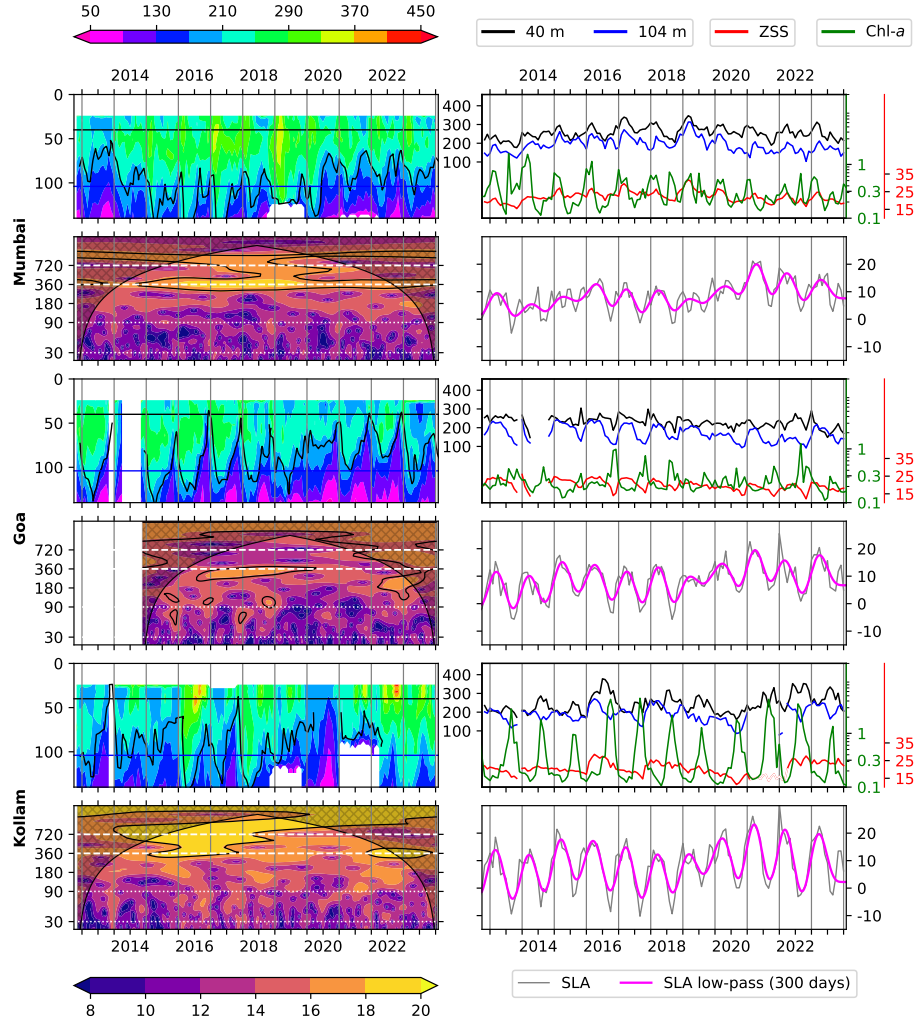


**Figure 9:** Decade-long biomass records off Mumbai, Goa, and Kollam are shown in the left panels. Black and blue lines indicate biomass at 40 m and 104 m, respectively; vertical grey lines separate years. Biomass is in units of  $\text{mg m}^{-3}$ . Below each record, wavelet power spectra of 40 m biomass are shown, with dashed white lines marking  $\sim 720$  and  $360$  days, and dotted lines denoting the intraseasonal band ( $30\text{--}90$  days). The right panels show time series of biomass at 40 m (black) and 104 m (blue), alongside ZSS (red) and chl-*a* (green) for the respective locations. All time series are resampled to a monthly time axis. Sea level anomaly (SLA, grey) is shown adjacent to the wavelet panels, overlaid with its 300-day low-pass filtered signal (magenta).

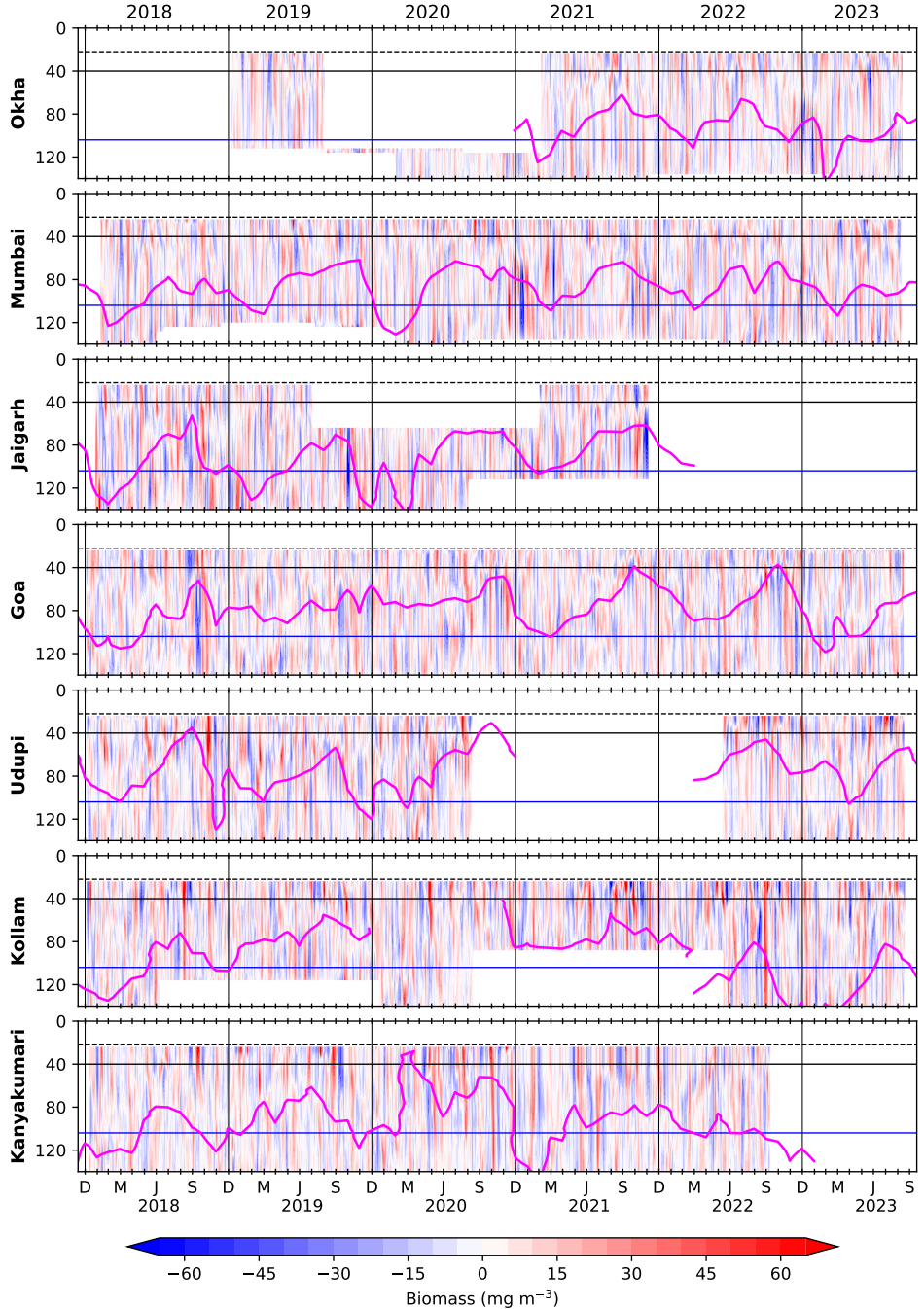


**Figure 10:** Biomass variation in the intraseasonal band (5–90 day period) is extracted using a Lanczos band-pass filter, capturing both high- and low-frequency intraseasonal components. Horizontal black and blue lines represent depths of 40 m and 104 m, respectively. Vertical black lines separate calendar years, and solid magenta curves indicate  $D215$  (or  $D175$  off Okha and Kanyakumari), derived from monthly biomass. The dashed line at 22 m marks the upper boundary of the first bin (centered at 24 m). Intraseasonal variability is evident throughout the time series and appears coherent along the slope, notably during October–December 2018.

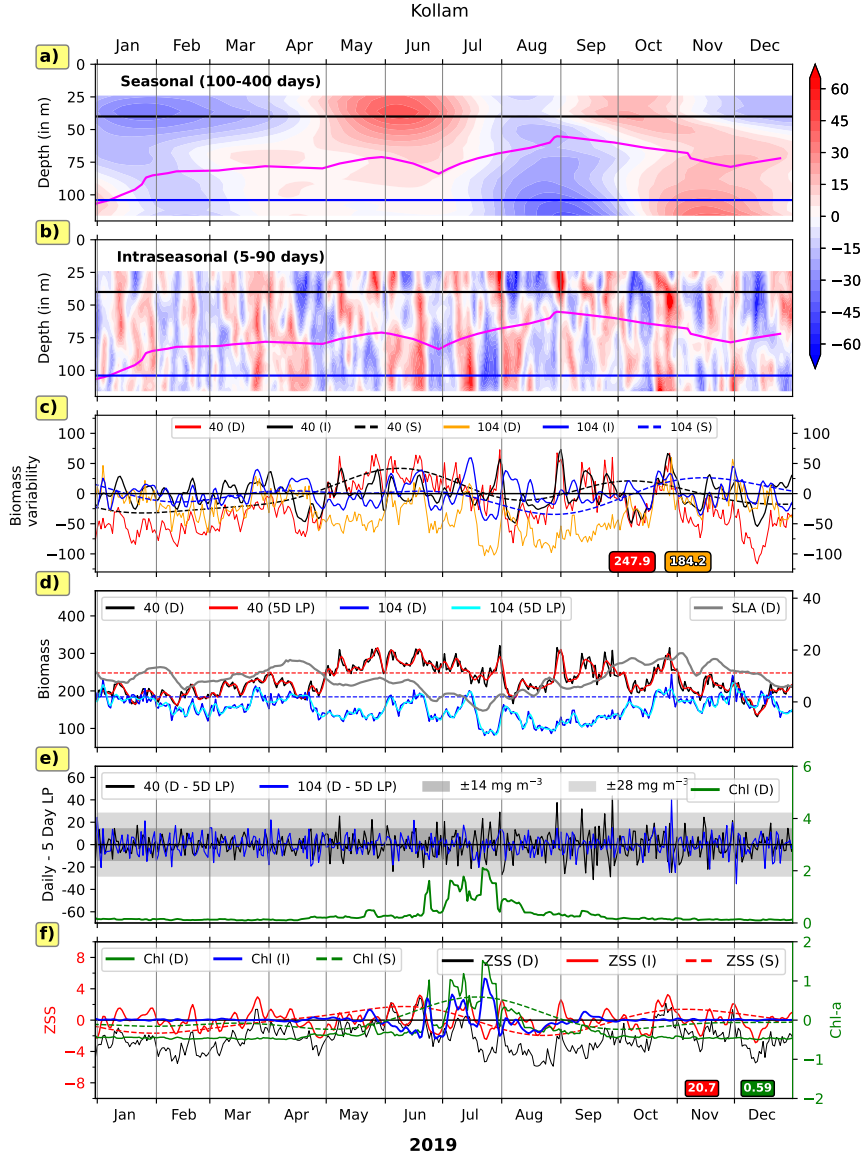


**Figure 11:** Figure consisting multiple plots showing the comparison of biomass variability in the seasonal and intraseasonal bands off Kollam. The top two panels display time-depth plots of seasonal and intraseasonal biomass on the same color scale. D215 is marked in magenta contours, depths of 40 m and 104 m are marked by black and blue lines, respectively, and vertical grey lines indicate month boundaries. The third panel from the top shows daily biomass at 40 m and 104 m, along with its intraseasonal (5–90 days) and seasonal (100–400 days) components. The mean daily biomass for each depth is noted in the bottom right corner of the panel. The fourth panel presents daily biomass overlaid with its 5-day low-pass filtered version and the daily sea level anomaly (SLA). Periods of high (low) SLA are observed to coincide with lower (higher) biomass at 40 m. The fifth panel shows the difference between daily and 5-day low-pass filtered biomass at 40 m and 104 m; grey and light grey shaded regions indicate the 1 standard deviation (SD) and 2 SD envelopes of the backscatter-to-biomass relationship, respectively, over which daily chl-*a* is overlaid. The bottom panel presents chl-*a* and ZSS in the intraseasonal and seasonal bands. See Figs. S4–S9 for a detailed comparison of variability across frequency bands.